JAMES | Journal of Advances in Modeling Earth Systems

RESEARCH ARTICLE
10.1029/2022MS003249

Special Section:
Using radiative-convective equilibrium to understand convective organization, clouds, and tropical climate

The Impact of a Land-Sea Contrast on Convective Aggregation in Radiative-Convective Equilibrium

Beth Dingley[1], Guy Dagan[2], Philip Stier[1], and Ross Herbert[1]

[1]Atmospheric, Oceanic and Planetary Physics, Department of Physics, University of Oxford, Oxford, UK, [2]The Hebrew University of Jerusalem, Jerusalem, Israel

Key Points:

- Convection preferentially aggregates over land in a global radiative-convective equilibrium simulation
- A global land-centered circulation drives the aggregation and is triggered through surface fluxes, but maintained through longwave fluxes
- The land-based convective cluster appears to have a maximum spatial scale of $\mathcal{O}$(10,000 km)

Supporting Information:

Supporting Information may be found in the online version of this article.

Correspondence to:

B. Dingley,
elisabethdingley@gmail.com

Citation:

Dingley, B., Dagan, G., Stier, P., & Herbert, R. (2023). The impact of a land-sea contrast on convective aggregation in radiative-convective equilibrium. *Journal of Advances in Modeling Earth Systems*, *15*, e2022MS003249. https://doi.org/10.1029/2022MS003249

Received 10 JUN 2022
Accepted 24 MAR 2023

Author Contributions:

Conceptualization: Beth Dingley, Philip Stier, Ross Herbert
Formal analysis: Beth Dingley
Investigation: Beth Dingley, Guy Dagan
Methodology: Beth Dingley
Visualization: Beth Dingley

Abstract Convective aggregation is an important atmospheric phenomenon which frequently occurs in idealized models in radiative-convective equilibrium (RCE), where the effects of land, rotation, sea surface temperature gradients, and the diurnal cycle are often removed. This aggregation is often triggered and maintained by self-generated radiatively driven circulations, for which longwave feedbacks are essential. Many questions remain over how important the driving processes of aggregation in idealized models are in the real atmosphere. We approach this question by adding a continentally sized, idealized tropical rainforest island into an RCE model to investigate how land-sea contrasts impact convective aggregation and its mechanisms. We show that convection preferentially forms over the island persistently in our simulation. This is forced by a large-scale, thermally driven circulation. First, a sea-breeze circulation is triggered by the land-sea thermal contrast, driven by surface sensible heating. This sea-breeze circulation triggers convection which then generates longwave heating anomalies. Through mechanism denial tests we find that removing the longwave feedbacks reduces the large-scale effects of aggregation but does not prevent aggregation from occurring, and thus we highlight there must be another process aiding the aggregation of convection. We also show, by varying the island size, that the aggregated convective cluster appears to have a maximum spatial extent of $\mathcal{O}$(10,000 km). These results highlight that the mechanisms of idealized aggregation remain relevant when land is included in the model, and therefore these mechanisms could help us understand convective organization in the real world.

Plain Language Summary Large tropical storm clouds can cluster together to form organized systems, which are associated with extreme precipitation within the cloudy region, and very dry conditions away from the cloudy region. These systems, called organized deep convection, are often studied in simplified models of the atmosphere where the land, Earth's rotation, and variations in sea-surface temperature are removed. In this paper we take a step toward reality and look at how including a large, idealized island in a simplified model affects how convection clusters. We show that convective clouds group together over the land throughout our model simulations. We investigate the processes driving this and find that surface flux feedbacks dominate early in the simulations. The feedbacks maintaining the convective aggregation are more complex. We find there is an important role for the longwave feedbacks, but that there must be another necessary process also aiding the clustering process. Our results highlight that the processes in highly idealized modeling studies seem to be relevant in more realistic models, and thus could help us understand how convection organizes in the real world. However, we also conclude it is important that follow-up work investigates the remaining additional feedbacks to gain a more complete understanding.

1. Introduction

In the tropics, deep convection transports large amounts of water vapor and energy vertically, as well as playing an important role in setting the Earth's radiative budget and large-scale circulations. This deep convection can be organized on a range of scales, from mesoscale convective systems, up to planetary envelopes of convection like the Madden-Julian Oscillation (MJO) (Madden & Julian, 1994; Tobin et al., 2012). Organized systems like these provide a significant contribution to tropical precipitation and cloudiness, with a large fraction of precipitation extremes occurring during convective organization (Roca & Fiolleau, 2020). Increased convective clustering has also been shown to affect large-scale circulations, including the structure and extent of the intertropical convergence zone (Popp & Bony, 2019).

Writing – original draft: Beth Dingley
Writing – review & editing: Beth Dingley, Guy Dagan, Philip Stier, Ross Herbert

Idealized climate models are a useful tool for studying moist convection in the tropical climate. In these models rotation, land, the diurnal cycle, and sea surface temperature (SST) gradients are often removed. In this simplified configuration, any imbalances caused by radiative cooling is balanced by convective heating. This balance is known as radiative-convective equilibrium (RCE) (Manabe & Wetherald, 1967). Removing these complexities associated with heterogeneities in the boundary conditions allows for studies to analyze the processes of importance to moist convection, such as its interactions with radiation and circulations (Wing et al., 2020). Due to the negligible Coriolis force in the tropics, previous studies have found that RCE is a reasonable representation of the tropical climate (Jakob et al., 2019), and therefore it has been extensively used in studies on the tropical atmosphere (e.g., Held et al., 1993; Khairoutdinov & Emanuel, 2013; Manabe & Wetherald, 1967; Robe & Emanuel, 2001; Stephens et al., 2008; Tompkins & Craig, 1998; Wing et al., 2020).

In many models using an RCE configuration, deep convection has often been found to spontaneously cluster together through radiatively driven circulations, despite homogeneous boundary conditions; a phenomenon called convective self-aggregation (Bretherton et al., 2005; Coppin & Bony, 2015; Held et al., 1993; Muller & Held, 2012; Tompkins & Craig, 1998; Wing & Emanuel, 2014; Wing et al., 2020). The self-aggregation of convection has been found to require longwave radiative feedbacks for its initiation and maintenance, with shortwave and surface enthalpy feedbacks being shown to contribute to the aggregation's initiation, but ultimately have been found not to be essential for aggregation to form (Coppin & Bony, 2015; Muller & Held, 2012; Wing & Emanuel, 2014; Yang, 2018a).

Despite RCE being regarded as a reasonable simplification of the tropical climate, the real world relevance of the behavior of deep convection in these models is debated. In particular, many of the processes which are removed in an RCE model have been shown to influence the organization of convection, such as SST gradients (Müller & Hohenegger, 2020; Shamekh et al., 2020a; Tompkins & Semie, 2021) and land-sea contrasts (Cronin et al., 2015; Leutwyler & Hohenegger, 2021; Sato et al., 2009). There are an increasing number of studies which highlight the possible role of the feedbacks essential to aggregation in real world convective processes. For example, both the MJO and tropical cyclones have been simulated in RCE models with rotation (Arnold & Randall, 2015; Davis, 2015; Khairoutdinov & Emanuel, 2018; Muller & Romps, 2018; Wing et al., 2016), and the diabatic heating from absorbing aerosol plumes has been shown to force convection to aggregate (Dingley et al., 2021). Inhomogeneous surfaces have also been shown to strongly affect convective aggregation. Studies have shown that SST gradients force convection to cluster over warmer SSTs (Müller & Hohenegger, 2020; Shamekh et al., 2020a; Tompkins, 2001a), whilst interactive SSTs have been shown to prevent or delay the aggregation of convection (Hohenegger & Stevens, 2016; Shamekh et al., 2020b; Tompkins & Semie, 2021). This is because the SST under a convective cluster will cool due to cloud shielding, whilst SSTs away from the convection will warm, which will then drive a circulation toward the dry region, disaggregating the convection. The organization of convection has also been studied on a land-like planet in RCE, with no ocean. Here Hohenegger and Stevens (2018) found that, as with interactive SSTs, the ability of land to change temperature causes a homogenization of the precipitation field on long time scales. They found that when an area of the domain is not covered by a convective cluster, the drying which occurs acts to induce a low-level circulation which changes the low-level flow direction toward this dry region, instead of toward the convective cluster. This clusters convection in this originally drier region, until a new dry area forms and induces this circulation reversal again. Therefore, these soil moisture-atmosphere interactions can act to prevent the long-term aggregation of convection.

Thus far, less attention has been given to the impact of land-sea contrasts on aggregation. Differences in the behavior of land and ocean could have large impacts on aggregation, such as the differences in the heat capacities of land and ocean (causing the land-ocean thermal contrast), moisture availability (land has the ability to dry out, whereas the ocean acts as an infinite water source), orography and the surface roughness length. Each of these factors can greatly affect the surface fluxes, which have previously been shown to impact the formation of aggregation (Bretherton et al., 2005; Coppin & Bony, 2015; Yang, 2018a), and so including land in RCE simulations could impact whether aggregation can form, and its lifetime, whilst also taking a large step toward a more realistic modeling paradigm.

Previous investigations of islands in an RCE model have shown that convection and precipitation tend to favor land (Coppin & Bellon, 2019; Cronin et al., 2015; Leutwyler & Hohenegger, 2021; Wang & Sobel, 2017). Land has also been found to have an impact on the domain-mean tropospheric temperature in an RCE simulation. Cronin et al. (2015) found that the presence of an island increased the tropospheric temperature comparatively to a aquaplanet simulation, and this warming increased monotonically with island size. They postulate that this is

due to the clouds forming at the warmest and moistest areas (which are over the island), pushing deep convection towards a moister adiabat. Contrastingly, Leutwyler and Hohenegger (2021) found that the presence of islands has a tendency to cool the troposphere, with larger islands having a larger cooling effect.

Hohenegger and Stevens (2018) discussed two pathways with which land, and the associated surface fluxes could influence the generation of circulations. The first was that moist soil favors convection (Findell & Eltahir, 2003; Gentine et al., 2013), creating a positive feedback where enhanced precipitation maintains soil moisture. The second pathway was that, if a soil moisture gradient can form, sensible heat gradients will also form, generating an opposing low-level circulation from moist to dry regions which can act to destabilize the convection (e.g., Taylor et al., 2012). In their work over a land-only planet, Hohenegger and Stevens (2018) found the latter pathway dominated, preventing the persistent aggregation of convection. Leutwyler and Hohenegger (2021) also attributed the ability of tropical islands to cool the troposphere in their simulations to the same mechanism and identified that this was the key difference between their work and the work of Cronin et al. (2015), where land was simply modeled as a patch of ocean with a heat capacity anomaly. This also links to known soil moisture versus radiation limited flux mechanisms—soil moisture limited regimes are those where the main control on evapotranspiration is the soil moisture, whereas radiation limited regimes are those when evaporative fraction is independent of soil moisture content (Seneviratne et al., 2010). Thus, with the more simplified set-up of Cronin et al. (2015), they are likely always in an energy-limited regime, whilst in the work of Hohenegger and Stevens (2018) and Leutwyler and Hohenegger (2021), soil moisture is providing a first-order control on evapotranspiration, and therefore surface fluxes will have a greater impact on the circulations.

The Tropical Rain belts with an Annual cycle and a Continent Model Intercomparison Project (TRACMIP, Voigt et al., 2016) devised another idealized modeling framework in order to investigate clouds, circulation and precipitation. In their project, simulations with a zonally symmetric, meridional SST gradient were performed which included a slab ocean and an idealized land continent. They find that adding a land continent led to a domain-mean cooling of 0.1–1.8K. In particular, Biasutti et al. (2021) found that the initial energy perturbation to the land surface leads to a significant warming of the continent, whilst in equilibrium the land warms at little at the equator, but the continent is mostly cooler than the surrounding ocean surface. The authors hypothesize that the local feedbacks between clouds and radiation are likely important at maintaining these surface temperature anomalies due to low atmospheric humidity.

Previous studies of islands in an RCE simulation have focused mainly on the effect the land-sea contrast has on the diurnal cycle, precipitation and temperature profile more than the mechanisms behind any organization of convection. They have also exclusively investigated the effect in a cloud-resolving model, where island size is limited. To our knowledge, no studies thus far have investigated the effect of a large, continentally sized island on aggregation. In this paper we aim to answer the following questions:

1. How does the inclusion of an idealized island in a global RCE model impact the aggregation of convection? In particular, the spatial structure of aggregation, and the domain-mean atmospheric properties.
2. How does the inclusion of an island affect the global circulation?
3. Are the physical mechanisms responsible for aggregation similar to those seen in land-free simulations, or forced aggregation simulations?
4. How sensitive are these results to the island size?

2. Methods

2.1. Model Set-Up

We employ the ICOsahedral Nonhydrostatic Atmospheric GCM (ICON, Giorgetta et al., 2018; Zängl et al., 2015), version 1.8, coupled to the JSBACH4 land model (Jungclaus et al., 2022) in all simulations described in this paper. This version of the ICON GCM model uses the ECHAM6 physics packages (for a full description, see Stevens et al. (2013)), including a bulk mass-flux convection scheme (Nordeng, 1994; Tiedtke, 1989) and cloud cover calculated using the relative humidity (Sundqvist et al., 1989). Other parameterization schemes used are the Lohmann and Roeckner microphysics scheme (Lohmann & Roeckner, 1996) and the gravity wave scheme as described in Stevens et al. (2013).

The JSBACH4 land model is a dynamic global vegetation model and offers a full representation of soil-vegetation-atmosphere interactions. The surface energy budget and soil thermal layers over land are implicitly coupled to

Table 1
Surface Properties Used to Initialize the JSBACH4 Land Model Within the ICOsahedral Nonhydrostatic Atmospheric GCM for the Rainforest and Grass Experiments

Parameter name	*Rainforest*	*Grass*
Soil type	Mixture of loam and clay (FAO flag 4)	Loam (FAO flag 3)
Plant functional type	4	7
Thermal diffusivity	$7.1 * 10^{-7}$ m^2 s^{-1}	$7.4 * 10^{-7}$ m^2 s^{-1}
Leaf area index	8.928	2
Root depth	1.351 m	1 m
Vegetation albedo	0.122	0.3
Roughness length	1.871 m	0.05 m
Soil depth (to bedrock)	2.194 m	3 m
Heat capacity	$2.36 * 10^6$ J m^{-3} K^{-1}	$2.25 * 10^6$ J m^{-3} K^{-1}
Heat conductivity	1.68 W m^{-1} K^{-1}	1.67 W m^{-1} K^{-1}
Soil porosity	0.456 m m^{-1}	0.459 m m^{-1}

ICON through the vertical diffusion scheme. There are four soil layers which descend to roughly 4.5 m depth; heat and water dynamics are defined on these soil levels.

ICON is run on a triangular grid, based on dividing a spherical icosahedron. In this paper we use the R02B04 grid, which has 20,480 cells, with an average cell area of approximately 25,000 km^2, and an approximate equivalent grid-spacing of 160 km. Each grid cell over land is divided into two sections: a "tiled" fraction, and the fraction of the non-ice covered grid-cell that is inhospitable to vegetation (e.g., rocky terrain or sandy desert). The tiled fraction of the grid box is then further separated into different surface types to represent sub-grid scale heterogeneity: a glacier, or one of 11 plant functional types (Reick et al., 2013). The vertical resolution is set by assigning 47 stretched model levels between the surface and model top at 83 km, with grid spacings ranging from 40 m between the lowest model layers, to around 1,350 m at 15 km, and 5,900 m near the model top.

2.2. Experimental Set-Up

ICON is used in an RCE configuration. The simulations are setup with no rotation, no diurnal cycle, no large-scale imposed winds, and a fixed SST of 305K, an SST where strong self-aggregation occurs in the ICON GCM (Dingley et al., 2021; Wing et al., 2020). The RCE state is initialized from homogenized boundary conditions with a solar insolation of 551.58 W m^{-2} and a fixed zenith angle of 42.05° giving a constant total insolation of 409.6 W m^{-2}, equivalent to the annual mean insolation in the tropics. The temperature and specific humidity profiles are initialized from a 1 month, non-aggregated aquaplanet simulation: we use horizontal means of the temperature and humidity profiles at the end of this non-aggregated simulation, and add some noise in the lowest five layers (see Wing et al. (2018)), then set those profiles as our initial conditions in the remaining simulations. The ocean albedo is set to 0.07. Concentrations of tracers CO_2, CH_4, N_2O, and O_2 are set to be constant in space and time and the O3 profile is the same as used in Popke et al. (2013). This atmospheric configuration follows that of the RCE model intercomparison (RCEMIP) project (Wing et al., 2018). In these simulations we use a model time step of 15 min, with radiation calculated every 90 min. The simulations described in this paper were run for 2 years.

Land in our simulations is represented by a large, circular island, located at latitude = 0° longitude = 0° with a radius of 40° (giving the land an area of 35.7*10^6 km^2). All land grid cells are completely covered by vegetation, with no glaciers. Surface properties have been set to average tropical rainforest-like values, with tropical broadleaf evergreen vegetation covering the island, to mimic tropical warm conditions. Rainforest surface properties are taken from the JSBACH4 initialization data set (Hagemann, 2002; Reick et al., 2021), and averaged over a box in the Amazon with latitudes ranging between −1° and −10° and longitudes ranging between −70° and −60°. Some of the key surface properties are listed in Table 1. Soil temperature is the only property not set using Amazon rainforest equivalent values. Soil temperature is initialized as equal to the SST at all model levels, following Leutwyler and Hohenegger (2021). We ran a test simulation with Amazon rainforest values for the soil

Table 2
List of Experiments

Experiment name	*Land*	*Interactive LW*	*Interactive SW*
Land-NoHomog	✓	✓	✓
Land-HomogLW	✓	×	✓
Land-HomogSW	✓	✓	×
NoLand-NoHomog	×	✓	✓
NoLand-HomogLW	×	×	✓

temperature and found that our results were invariant to this choice. Results were also tested with island surface temperatures ranging between 300 and 310K at increments of 1K, and again were found to be invariant to our choice of initial temperature. Another sensitivity test was performed for the vegetation type. For this test we changed from rainforest land parameters, to grass parameters (see Table 1). The results of this test were again, quantitatively similar to the rainforest experiment, and can be found in Appendix A. The island has an elevation of 0 m everywhere, to remove topographical effects on convection and its organization.

To test the impact of the radiative feedbacks on aggregation, we perform mechanism denial tests, where the longwave or shortwave radiative fluxes are horizontally homogenized in turn, at each model level and each time-step. These experiments will hereafter be referred to as Land-HomogLW and Land-HomogSW, respectively. Surface fluxes remain interactive for all simulations.

Finally, in order to contextualize our results with existing self-aggregation studies, we will compare our simulations to both an aggregated and a non-aggregated RCE simulation without land. Dingley et al. (2021) showed that, at an SST of 305K aquaplanet ICON GCM RCE simulations (that are otherwise identical to the above Land-NoHomog) strongly self-aggregate with interactive radiative fluxes, and do not aggregate with homogenized longwave radiative fluxes (see Figures 9g and 9h in Dingley et al. (2021), respectively). Thus, these are the simulations we will use to compare our results to (hereafter NoLand-NoHomog, and NoLand-HomogLW, respectively). A table describing all experiments in this paper can be found in Table 2.

2.3. Analysis Methods

In order to compare the relative degree of aggregation of different simulations, we use the variance of column-integrated relative humidity (CRH, σ^2_{CRH}) metric (Wing & Cronin, 2016). Column relative humidity (CRH) is defined as the ratio of the density-weighted integral of tropospheric water vapor and its saturation counterpart. This metric utilizes the signature of aggregation where moist regions moisten and dry regions get drier as convection clusters together, driving a broadening of the moisture distribution. This metric does not have a threshold value above which convection is considered as aggregated. Instead, it is used as a comparative metric which allows us to compare the relative degree of aggregation across different simulations. We also tested results using the variance of frozen moist static energy (FMSE). For all simulations, results were qualitatively similar.

To help us identify important feedbacks driving aggregation in our simulations, we will use the FMSE variance budget, as defined by Wing and Emanuel (2014). This method used the column-integrated FMSE:

$$\hat{h} = \int_{trop} \rho h dz = \int_{trop} \rho(gz + C_p T + L_v q_v - L_f q_{ice}) dz \tag{1}$$

as it is approximately conserved during convection with no ice phase surface precipitate. Here h is the FMSE, ρ is the air density, gz is the geopotential, C_p is the specific heat capacity of dry air, T is the air temperature, L_v is the latent heat of vapourization, L_f is the latent heat of fusion, and q_{ice} is the ice mixing ratio. $\int_{\text{trop}}$ indicates we are integrating over the troposphere. As convective aggregation increases, it broadens the moisture distribution and in tropical regions, increases in $\hat{h}$ are typically driven by increases in moisture (Sobel et al., 2001). Thus increases in convective aggregation are associated with increases in the spatial variance of $\hat{h}$. Following this, Wing and Emanuel (2014) derived a budget for the variance of FMSE:

$$\frac{1}{2}\frac{\partial \hat{h'}^2}{\partial t} = \hat{h'} SEF' + \hat{h'} NetLW' + \hat{h'} NetSW' - \hat{h'} \nabla_h \cdot \vec{u}\hat{h} \tag{2}$$

Here, primed quantities $[\cdot]'$ represent an anomaly from the global horizontal mean, SEF stands for surface enthalpy fluxes, which is the sum of the latent and sensible heat fluxes, NetLW and NetSW are the column longwave and shortwave radiative flux convergences respectively where:

$$NetLW = LW_{sfc} - LW_{toa} = \left(LW\uparrow_{sfc} - LW\downarrow_{sfc}\right) - LW\uparrow_{toa} \tag{3}$$

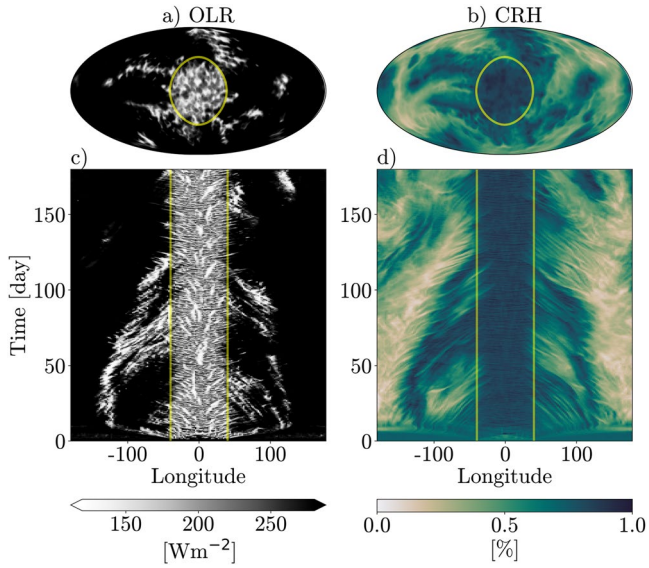

Figure 1. (a, b): Four-hour mean snapshots of (a) outgoing longwave radiation (OLR) and (b) column relative humidity (CRH) 180 days after simulation start. (c, d): Hovmöller plots of (c) OLR and (d) CRH over the first 180 days of the Land-NoHomog simulation, taken as a zonal slice through latitude = 0°. The yellow lines show the coasts of the 40° island.

$$NetSW = SW_{toa} - SW_{sfc} = (SW\downarrow_{toa} - SW\uparrow_{toa}) - (SW\downarrow_{sfc} - SW\uparrow_{sfc}). \quad (4)$$

$\hat{h}'\nabla_h \cdot \hat{\vec{u}h}$ is an advective term which is calculated as a residual from the rest of the budget. Each term on the right-hand side of Equation 2 represents a covariance with a source or sink of FMSE. Therefore, a positive term represents a positive feedback on aggregation.

3. Results

3.1. Land-Centered Aggregation

Convection primarily forms over the island throughout our Land-NoHomog simulation (Figures 1a and 1c), driving large moisture gradients, with the moistest columns of the domain consistently over the island, and the driest columns typically furthest away from the island (Figures 1b and 1d). This aggregated state is visually reached approximately between 5 and 10 days after the simulation start, although atmospheric equilibrium and therefore equilibrium in the moisture variance is reached approximately 70 days after simulation start (Figure 3). In Figure 1b we can see two modes of wave propagation—the first moves from land to sea soon after simulation outset. This will be discussed in more detail later in the manuscript. There is also evidence of slowly propagating convective packets moving from ocean to land from approximately day 50 onward. This is evident as the convection which forms over the ocean subsequently gets advected toward the island at roughly 3 m s^{-1}, and thus is likely a local moisture mode (see Grabowski and Moncrieff (2004) and Tompkins (2001b)). Convection which is triggered over the island itself, typically forms at the center of the island and is advected toward the coastline of the island. Videos of the outgoing longwave radiation (OLR) and CRH over the first 6 months can be seen in Movie S1.

We earlier introduced the two pathways with which land, and the associated surface fluxes could influence the generation of circulations from Hohenegger and Stevens (2018). Namely, a soil moisture-limited regime where the main control on evapotranspiration is the soil moisture, or a radiation-limited regime where the evaporative fraction is independent of soil moisture. In our simulations, despite the use of a dynamic vegetation model where soil moisture gradients could form, the persistent cluster of cloud covering the island prevents this, and thus we remain in the radiation-limited pathway, where evaporation is not limited by soil moisture (Koster et al., 2004; Seneviratne et al., 2006, 2010). This is evident from Figure 2, where we can see that the relative soil moisture (mostly) increases in all soil layers from the start of the simulation. After approximately 50 days, the soil column is almost completely saturated. The water budget is balanced in this model through surface runoff, drainage at the bottom of the soil column, and a small surface water convergence. In this simulation, there is approximately 1 mm of surface water for most of the simulation, and with the rainforest vegetation type, drainage provides the largest moisture sink. Thus, despite the more advanced modeling configuration, our island becomes closer to the saturated island simulation of Cronin et al. (2015).

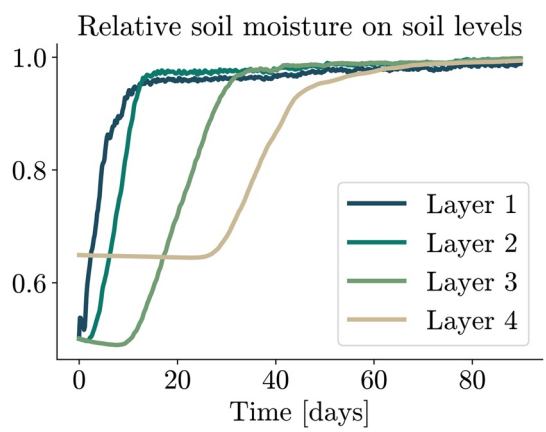

Figure 2. Timeseries of the soil moisture, relative to field capacity in each of the four soil layers over the first 90 days of the Land-NoHomog simulation. Layer 1 is the surface layer (0–0.065 m), layer 2 (0.065–0.319 m), layer 3 (0.319–1.232 m), and layer 4 (1.232–4.134 m).

Figure 3 shows a comparison of the domain-mean properties of this simulation (Land-NoHomog) with the NoLand-HomogLW simulation, and the NoLand-NoHomog simulation. We can see that comparatively to the NoLand-HomogLW simulation, there is a strong domain-mean warming, free-tropospheric drying, and a decrease in high level clouds. This is consistent with the results of many previous self-aggregation studies (e.g., Cronin & Wing, 2017; Wing et al., 2020). The Land-NoHomog shows similar domain-mean effects of aggregation to the NoLand-NoHomog simulation, with Figure 3a showing the same degree of aggregation between these two simulations. There is also little change in the amount of free-tropospheric drying and reduction in high cloud fraction between the runs with/without

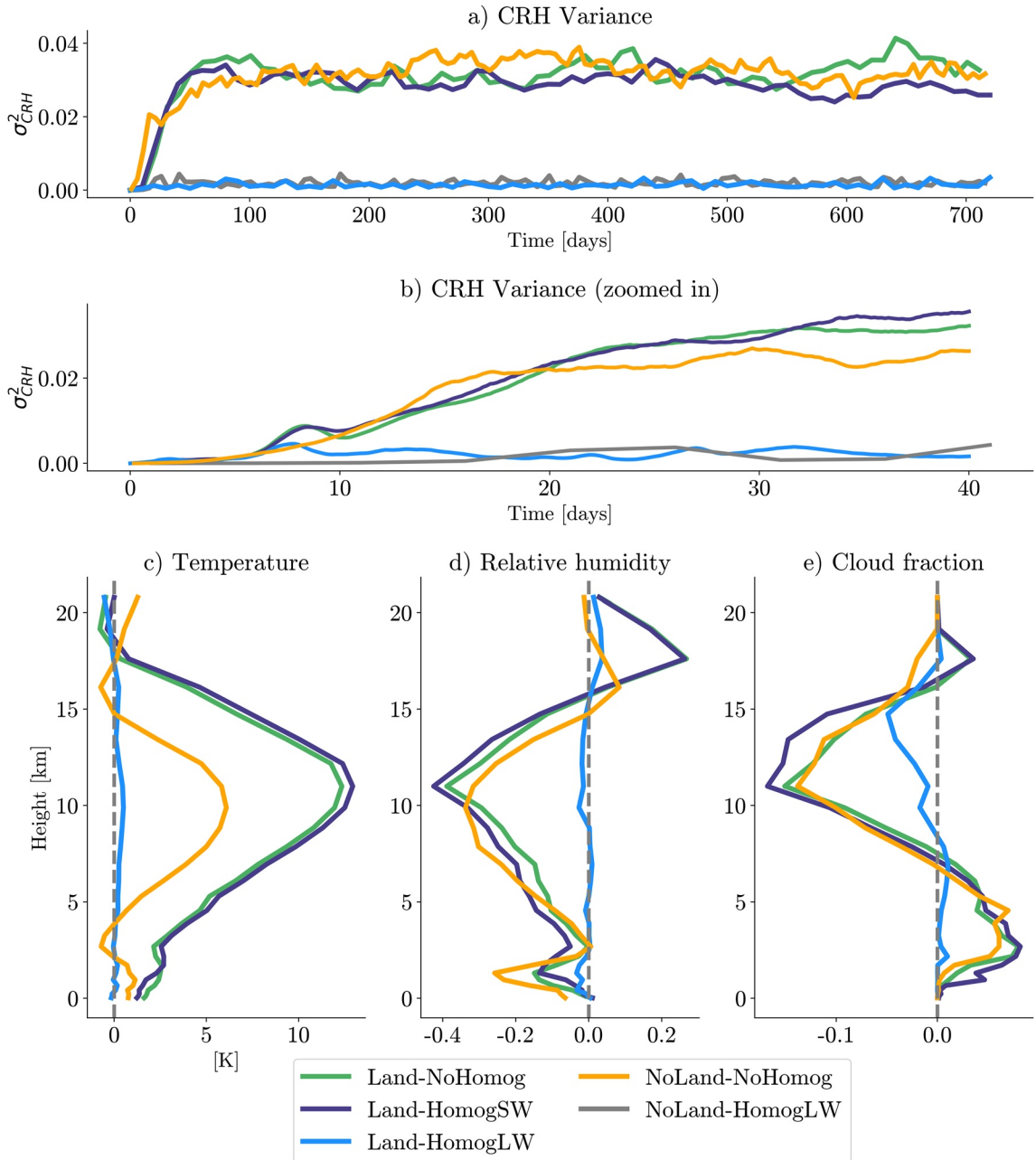

Figure 3. (a, b) Time evolution of variance of domain-mean column relative humidity (σ^2_{CRH}). (c–e): Domain-mean vertical profiles of (c) temperature, (d) relative humidity, (e) cloud fraction, difference from NoLand-HomogLW, time-averaged over days 100–720 of the simulations.

land, but there is slightly less drying of the lower troposphere and an increase in tropopause height when land is present. Despite these similarities between the simulations with/without land, there is a much stronger domain-mean warming throughout the troposphere in the Land-NoHomog simulation. This would happen if the convection in the simulation with land is on a warmer moist adiabat than the convection in the simulation without land. This is true in our simulations as the Land-NoHomog has convection forming over a warmer lifting condensation level than the NoLand-NoHomog experiment. Our result here agree with Cronin et al. (2015), but not with Leutwyler and Hohenegger (2021), as would be expected from the soil moisture analysis above.

It is clear from Figure 1 that there is a large-scale circulation being generated and maintained over the island in the Land-NoHomog simulation, and that this is likely responsible for the aggregation of convection throughout our simulation. It has been shown before that the self-aggregation of convection is generally driven by self-generated

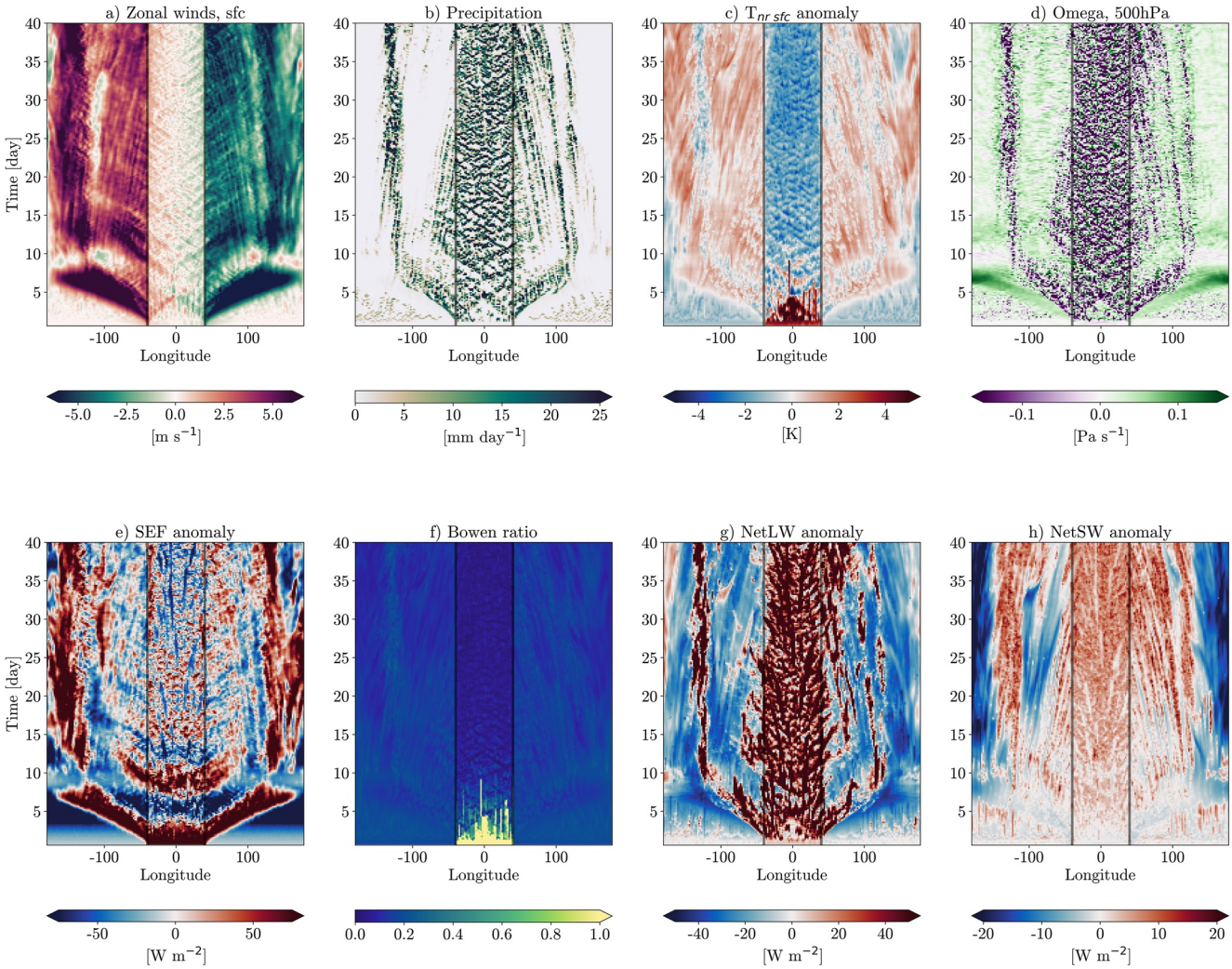

Figure 4. Hovmöller plots of (a) Surface zonal winds, (b) Precipitation, (c) Near-surface temperature anomaly, (d) Omega at 500 hPa, (e) surface enthalpy flux (latent heat flux [LHF] + sensible heat flux [SHF]) anomaly, (f) Bowen ratio (SHF/LHF), (g) NetLW anomaly, and (h) NetSW anomaly, over the first 40 days the Land-NoHomog simulation, taken as a zonal slice through latitude = 0°. The black lines show the coasts of the island. NetLW and NetSW are the column longwave and shortwave radiative flux convergences, respectively. Anomalies are calculated from the horizontal mean.

radiative circulations. These circulations have often been shown to start as an anomalous patch of dry sky, which then grows and pushes the convection to cluster together (Coppin & Bony, 2015; Holloway & Woolnough, 2016; Muller & Bony, 2015; Muller & Held, 2012), a mechanism for which longwave radiative feedbacks are generally essential both for triggering and maintenance. We investigate here whether the convection is aggregated through the same mechanisms as self-aggregation. We will study this first by discussing the thermodynamics responsible for triggering the circulation, and then for maintaining the circulation.

Figure 4 shows some of the key physical quantities driving the circulation over the first 40 days of our simulation. Figure 4a illustrates the aforementioned circulation, and its extent. We can see that the surface winds are converging toward the island at every oceanic point, with approximate speeds of 3 m s^{-1} once aggregation has been reached (roughly 10 days after simulation start). This circulation is being triggered initially by very strong SHF spatial anomalies as indicated by a strongly positive SEF spatial anomaly in Figure 4e and a Bowen ratio above one in Figure 4f at the start of the simulation. This drives high near-surface temperature spatial anomalies which cause strongly negative boundary layer density anomalies, and hence positively buoyant air over the island. The land-sea thermal contrast also causes surface winds. The circulation described here is analogous to the well documented sea-breeze circulation (Miller et al., 2003), which subsequently triggers convection (Carbone et al., 2000; Crook, 2001; Kingsmill, 1995). The convection starts at the edge of the island, and as the surface circulation

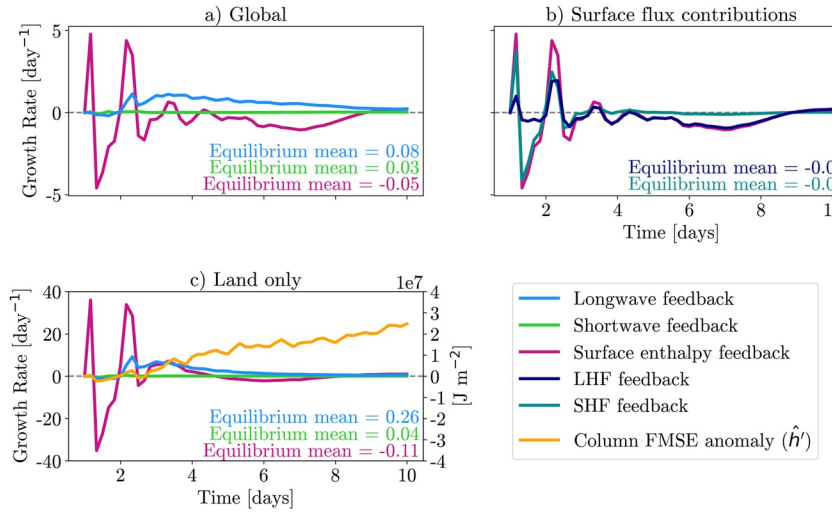

Figure 5. Timeseries of diabatic terms in frozen moist static energy variance budget (Equation 2) over first 10 days of the Land-NoHomog simulation. (a) Averaged globally, (b) Globally averaged surface flux contributions, and (c) averaged over the island only. Panel (c) also includes the land-averaged values of $\hat{h}'$, on the right-hand y-axis. Light blue lines show longwave feedback, green lines show shortwave feedback, pink lines show surface enthalpy feedback, navy blue lines shown latent heat flux feedback, teal lines show sensible heat flux feedback, orange line shows $\hat{h}'$. Mean values over days 90–180 (when the simulation is in equilibrium) of each feedback are given in the text on each plot (color of text corresponds to feedback line color).

grows in strength, moves inwards until the whole island is covered by convecting air (Figure 4d). For a more zoomed in version of Figure 4, please see Figure S1 in Supporting Information S1. These results highlight that boundary layer processes are likely important for the initiation of aggregation, supporting recent results from other studies (e.g., Muller & Bony, 2015; Naumann et al., 2017; Yang, 2018a, 2018b). In particular, Muller and Bony (2015) showed that the boundary layer advection of FMSE was vital for the self-aggregation of convection. We will show later in the manuscript that this process is also a key driver of aggregation in these simulations.

The convection over the island triggers a gravity wave propagating at 30 m s^{-1} at 500 hPa, which acts to eliminate horizontal density gradients in the free-troposphere. This gravity wave is responsible for propagating the temperature of the warmer moist adiabat that the convection is on to the rest of the domain, consistent with the weak temperature gradient approximation (Leutwyler & Hohenegger, 2021; Sobel et al., 2001). Evidence of this wave can be seen in Figure 4, especially in Figure 4d as a wave of subsiding air moving outwards away from the island, and in the timescale of the inward-moving convection over the island in the initial triggering phase (Figure 1c). The subsidence associated with this wave causes a strong drying of the columns far away from the island (Figure 1d), which completes the process of aggregation. Figures 4g and 4h show that in the initial 2 day period during which this circulation is being spun-up, the horizontal anomalies in both column longwave and shortwave radiative fluxes are minimal. Thus, it seems from Figure 4 that the circulation which aggregates the convection is triggered in this simulation with land primarily through surface fluxes, mostly the SHF. Once the convection starts to form, the longwave radiative spatial anomalies grow, implying that longwave feedbacks play an important role in our circulation, but are less important for the circulation to be triggered initially.

If we investigate the feedbacks in the first 10 days through the FMSE variance budget method, we can see similar results (Figure 5). For all feedbacks, the values are driven primarily by the value of the feedbacks over land, therefore we also show the feedbacks averaged over the land tiles only (Figure 5c). In the first 3 days, the surface enthalpy feedback is the dominant term driving FMSE variance with the SHF feedback providing the largest contribution (Figure 5b). Both the globally averaged and land-averaged term oscillate between positive and negative values. This is due to the oscillation in the land-averaged $\hat{h}'$ term. The sign of the surface enthalpy flux horizontal anomaly, however, remains positive (Figures 4e and 4f), acting as a source of FMSE over the island consistently in the first 3 days of the simulation. Thus, we argue that the surface fluxes drive the aggregation of convection over land in the earliest days of our simulation. After 2 days, the longwave feedback begins to increase, and it becomes the dominant positive feedback after 3 days of simulation. The contribution from

the longwave feedback then remains the dominant feedback throughout the remainder of the simulation. This is in agreement with the analysis above, where we identified that horizontal anomalies in the column longwave radiative flux convergence over land are large and positive after the initial triggering of the circulation. Thus, the FMSE variance budget feedback decomposition analysis supports our conclusion that it is the surface fluxes which are primarily responsible for triggering the aggregation processes, but the longwave feedbacks become increasingly important, and remain the strongest positive feedback in the equilibrium feedback.

After this initial aggregating period, convection remains persistently over the island (Figures 1c, 1d, 4b, and 4d). A key difference between the land model and atmospheric model is that the land surface energy budget is closed, whilst the ocean surface energy budget is not. This means that the land surface can change temperature, whilst the ocean temperature is fixed. Thus, once convection has formed, due to shortwave cloud shielding, the land surface temperature cools (Figure 4c—note that this is near surface temperature, but reflects the behavior of the surface temperature). This surface cooling, combined with the saturated soil, leads to a very low Bowen ratio over the island significantly reduced sensible heat fluxes locally. Despite this cold land temperature, the surface zonal winds (Figure 4a) show that the circulation does not reverse toward the now warmer ocean anomalies, and convection remains aggregated. To investigate the mechanisms driving this equilibrium stage of our simulation, we analyze time-averaged, longitude-height plots of various physical quantities (Figure 6). Figure 6a again shows the global circulation that is keeping the convection aggregated together, that is, surface convergence toward the island center with strong upper tropospheric divergence away from the island. Figure 6b shows the vertical motions associated with convection, and Figures 6c and 6d show the aggregated moisture and cloud water content fields. Importantly, the surface convergence allows for an advection of high surface FMSE toward the convective cluster (Figure 6e), which has previously been shown to be an important process driving aggregation (e.g., Muller & Bony, 2015; Muller & Held, 2012).

Inspecting the horizontal virtual temperature anomalies in Figure 6f reveals that the near-surface negative temperature anomalies in Figure 4c are confined to less than 500 m above the surface. Above this, there is still a temperature gradient with warmer anomalies over the island than ocean, and therefore the circulation aggregating the convection is still being thermally driven. However, initially this circulation was being driven by the land-sea thermal contrast caused by the land surface heating up. This poses the question, what is now driving the thermal anomalies over the island? Figure 6h illustrates the strong gradients in longwave flux convergence anomalies in the lower troposphere, which are positive over the island and negative away from the island. These gradients drive the temperature gradient in Figure 6f and are responsible for driving the maintenance of the global circulation. This mechanism is the same as is discussed in previous studies (e.g., Wing et al., 2017). The shortwave heating anomalies also show a pattern one would expect—negative anomalies in the lower troposphere representing the effects of cloud shielding and positive anomalies in the upper troposphere due to absorption by water vapor. However, the overall horizontal radiative heating anomaly pattern is driven by the longwave radiative feedbacks (Figure 6j). These results agree with the conclusions from the FMSE variance budget analysis, which showed that the longwave feedbacks, especially those over the island, are the strongest mechanism drive aggregation in the equilibrium stages of our simulation (Figure 5). We therefore suggest that longwave feedbacks are important for maintaining the island-centered circulation and therefore maintaining the aggregation of convection over the island.

3.2. Mechanism Denial Tests: Can Land Aggregation Occur in the Absence of Horizontal Radiative Flux Anomalies?

In order to test our radiative heating hypothesis, we analyze the results from our mechanism denial tests. These tests allow the radiative heating rates to change through time, but remove the horizontal gradients, thought to be responsible for maintaining the aggregation of convection. Figure 3a shows that homogenizing the shortwave fluxes has had little impact on the overall degree of aggregation, whereas homogenizing the longwave fluxes has decreased the degree of aggregation to the same as the NoLand-HomogLW experiment. If we inspect the first 40 days of the simulations more closely (Figure 3b) then we can see that the CRH variance increases similarly in the first 7 days of each simulations with land, then it is after this that the degree of aggregation drops in the Land-HomogLW simulation. This supports the findings in the previous section that the surface fluxes are driving the spin up of the circulation, with longwave feedbacks taking over as an important feedback after this.

Additionally, in the domain-mean vertical profiles of temperature, relative humidity, and cloud fraction (Figures 3c–3e), the Land-HomogSW simulation mirrors the Land-NoHomog simulation, and the

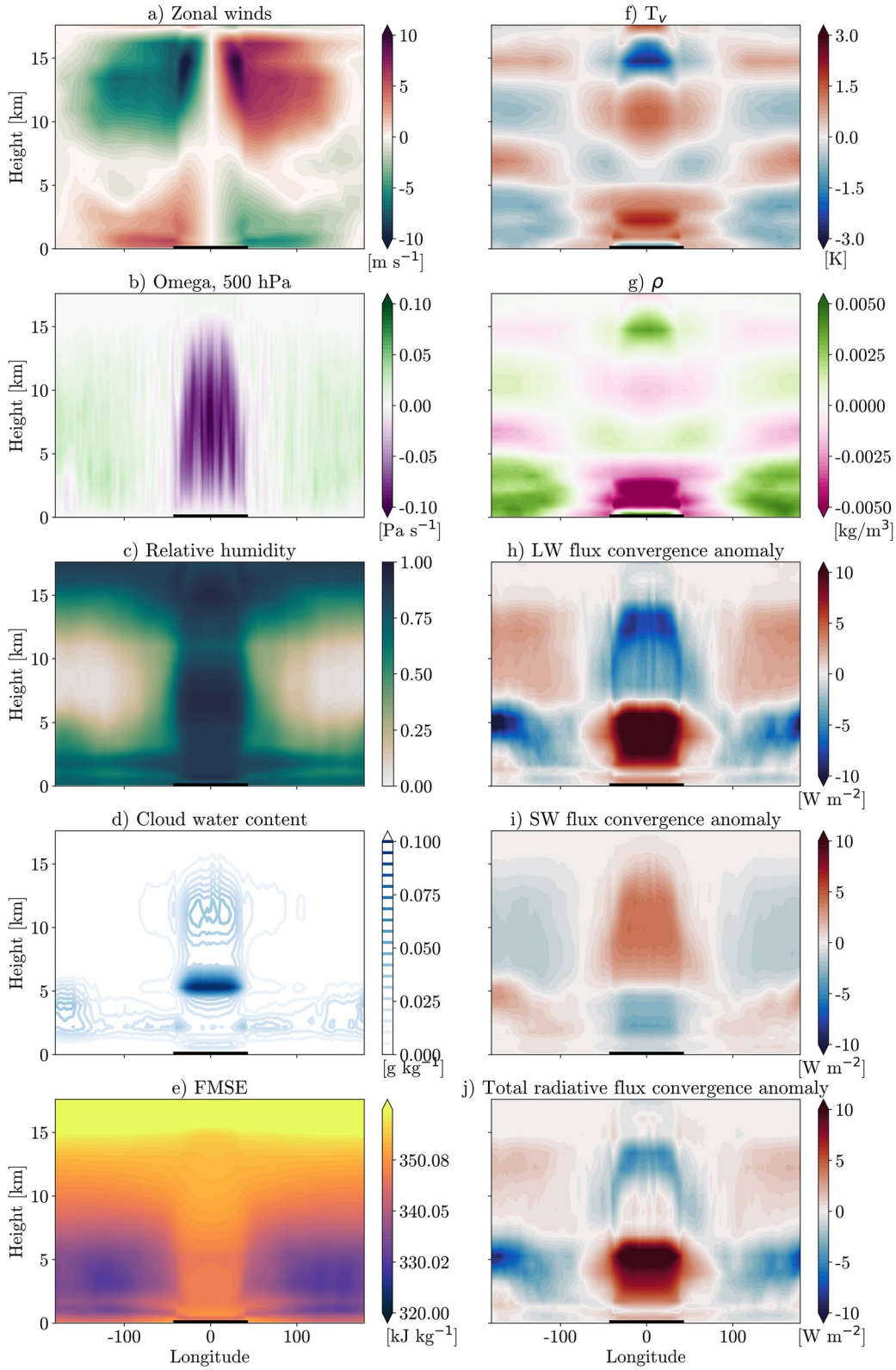

Figure 6. (a) Zonal winds, (b) Omega, (c) Relative humidity, (d) Cloud water content, (e) frozen moist static energy, (f) Virtual temperature anomaly, (g) Density anomaly, (h) Longwave radiative heating anomaly, (i) Shortwave radiative heating anomaly, and (j) Total radiative flux convergence anomaly. Plots are zonal slices taken at latitude = 0°, averaged over days 100–720 of the Land-NoHomog simulation. Island is located between longitudes ±40°, as indicated by thick black line. Anomalies are calculated from the horizontal mean.

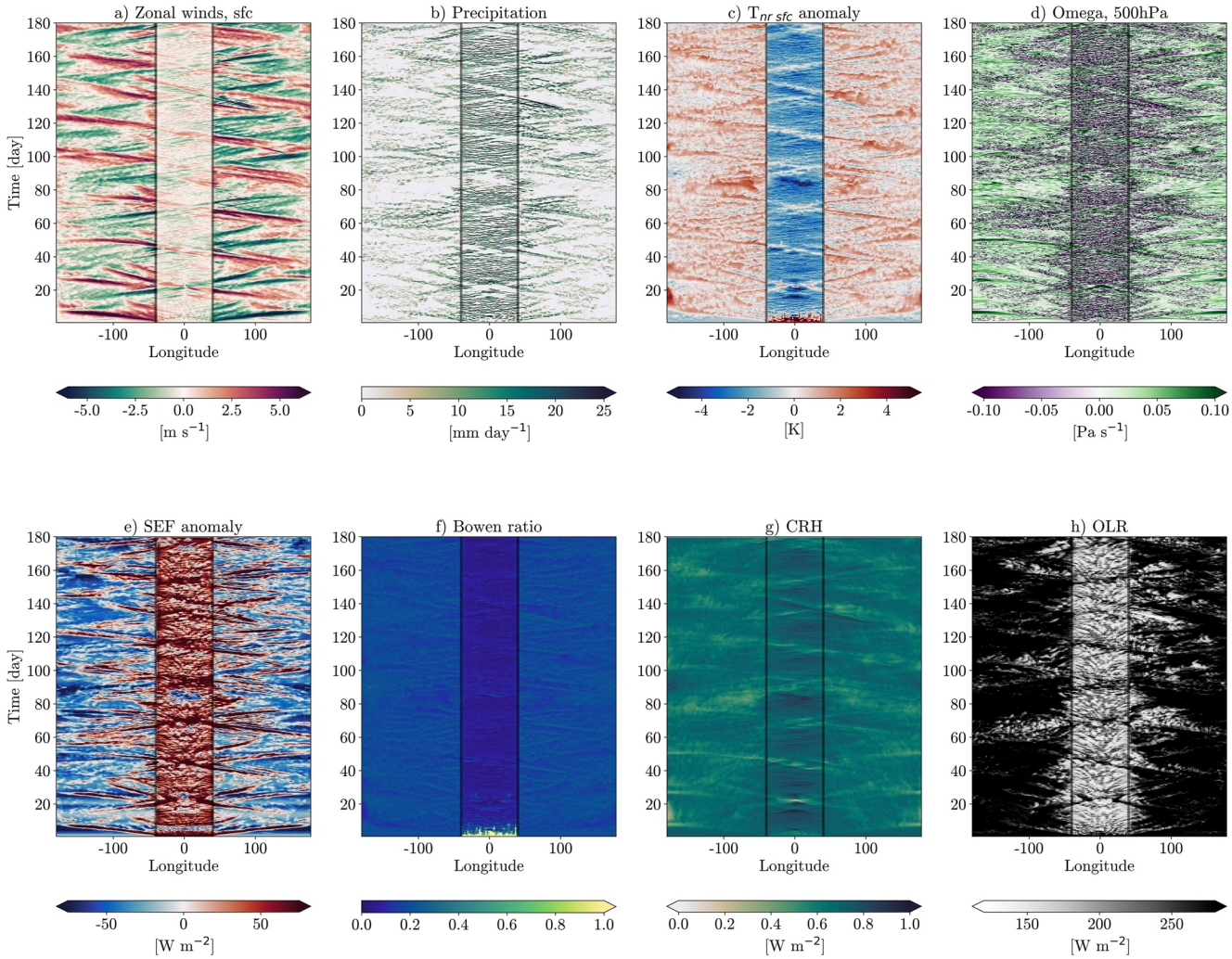

Figure 7. Hovmöller plots of (a) Surface zonal winds, (b) Precipitation, (c) Near-surface temperature anomaly, (d) Omega at 500 hPa, (e) Surface enthalpy flux (latent heat flux [LHF] + sensible heat flux [SHF]) anomaly, (f) Bowen ratio (SHF/LHF), (g) Column relative humidity, and (h) Outgoing longwave radiation, over the first 180 days of the Land-HomogLW simulation, taken as a zonal slice through latitude = 0°. The black lines show the coasts of the island. Anomalies are calculated from the horizontal mean.

Land-HomogLW simulation mostly mirrors the NoLand-HomogLW simulation. This also implies that the large domain-mean effects in Land-NoHomog discussed earlier are due to the aggregation process, not due to the inclusion of land itself.

The results from Figure 3b suggest that the circulation that is triggered in Figure 4 would also be triggered in the absence of longwave feedbacks, but that it is not being maintained, as we are seeing less impact of aggregation on the moisture distribution, domain-mean cloud fraction, and temperature. Indeed, if we study Hovmöller diagrams of the Land-HomogLW simulation (Figure 7) we can see that this appears to be true. The same circulation spin up can be seen by the land-sea thermal contrast in Figure 7c, and the subsequent gravity wave of subsidence in Figure 7d, however, without the convection triggering longwave feedbacks over the island, this circulation is not maintained, and instead the horizontal motion is now being dominated by wave-like motions across the globe (Figure 7a). This wave also travels at roughly 30 m s^{-1}, as in our original simulation. These waves travel away from the island, passing through each other at the island's antipode, creating a surface circulation which alternates between land-centered and ocean-centered and repeats periodically approximately every 15–25 days. At the points of strongest surface-level divergence away from the island (e.g., around day 20 in Figure 7a), the surface windspeeds over land increase, creating a warm, dry anomaly over the center of the island, above which there is clear-sky (Figure 7h). This point dries due to the increased windspeeds and the subsidence associated with

the diverging circulation, and warms because of the increased surface shortwave absorption due to the clear-sky above as well as the increased windspeeds again. This warm anomaly then triggers new convection, resulting in the same thermally driven circulation and subsequent gravity wave mechanism discussed. This wave-like motion across the atmosphere is illustrated in Movie S2 of OLR and CRH. These results were also tested for simulations which were started from the equilibrium aggregated state shown in Figure 1, and then had the longwave heating rates homogenized. The results for this were the same as in Figures 3 and 7, and can be seen in Figure S2 in Supporting Information S1.

From the precipitation, vertical pressure velocity, and OLR fields (Figures 7b, 7d, and 7h), convection is less organized throughout the Land-HomogLW simulation than in our original Land-NoHomog simulation, due to an increase in oceanic convection. However, over the island we still see persistent convection, as in the Land-NoHomog simulation, except during the brief suppression period at the peak of the ocean-centered circulation. Therefore, there is clearly another mechanism responsible for organizing convection over land other than the longwave radiative fluxes. However, this mechanism is not driving the same level of moisture variance as in our Land-NoHomog simulation.

To further understand this we again consider longitude-height slices of the equilibrium circulation, in Figure 8. The surface zonal winds in Figure 7a showed that there was no longer a large-scale, land-centered circulation being maintained in the Land-HomogLW simulation. However, Figure 8a shows that there is still a large-scale overturning circulation, but it no longer extends to the surface. We now have land-centered convergence starting at approximately 4 km, with similar upper-tropospheric outflow as in Land-NoHomog. The structure of the virtual temperature anomaly has also changed—the large positive anomaly in the lower troposphere in Land-NoHomog has been significantly weakened and the strongest horizontal anomaly in Land-HomogLW is now between 7 and 10 km, driven by the shortwave heating anomaly (Figure 8i). The driving feedback thus combines these results: island-based convection will have upper-tropospheric outflow, which must re-converge due to mass conservation. This convergence is toward the strongest virtual temperature anomaly, which is elevated in comparison to the Land-NoHomog simulation. Therefore, gravity-wave dominated, horizontal winds in the boundary layer are somewhat disconnected from this large-scale overturning circulation, although the gravity wave motion still impacts the zonal winds at higher altitudes with wave speeds superimposed on the background large-scale circulation. This elevated large-scale circulation also means that the advected FMSE is of much lower energy, therefore acting as a negative feedback on aggregation in the Land-HomogLW simulation. Thus, these results indicate that near-surface advection of FMSE is possibly the key for convective aggregation to affect the energy budget by driving a broadening of the moisture distribution, supporting the results of Muller and Held (2012) and Muller and Bony (2015).

3.3. Sensitivity to Island Size

In order to test our results' sensitivity to the island size, we ran an ensemble of simulations where the island radius was increased from 10° to 80° in 10° increments. The winds, near-surface temperature, OLR and CRH Hovmöller plots for these experiments are shown in Figure 9. The standard result we've seen in this study, that convection will preferentially form over the island, forced by a large thermally driven circulation mostly holds at all island sizes. The extent of the circulation is much smaller in the 10° island simulation, as are the maximum horizontal windspeeds. This circulation extent grows, reaching across almost the whole globe in the simulations with island sizes between 20° and 50°. Along with this the convective cluster also grows to cover the whole island, leading to cool near-surface temperature anomalies over the island, due to the cloud shielding effect. Interestingly, above 50° the circulation stops growing in extent, and the convective cluster stops growing in size. At 60°, 70°, and 80° the convective cluster stays mostly the same size as the cluster in the 50° simulation, and so is no longer covering the whole island. This results in clear sky patches around the convective cluster, leading to large near-surface temperature anomalies. There is also a reduction in the horizontal extent of the zonal winds. We speculate that these results could point to a maximum size of aggregation cluster which would cover approximately 20% of the globe. Indeed, if we calculate the average fraction of the globe which is convecting by dividing the area of the domain that has a negative vertical pressure velocity (ω) by the total domain area, we find that approximately 25% of the globe is convecting at all times in all of the simulations once aggregated. Thus, the island is not causing an increase in the amount of convection, but simply determining the locations at which convection preferentially forms. In the largest island simulations, when there is very little convection

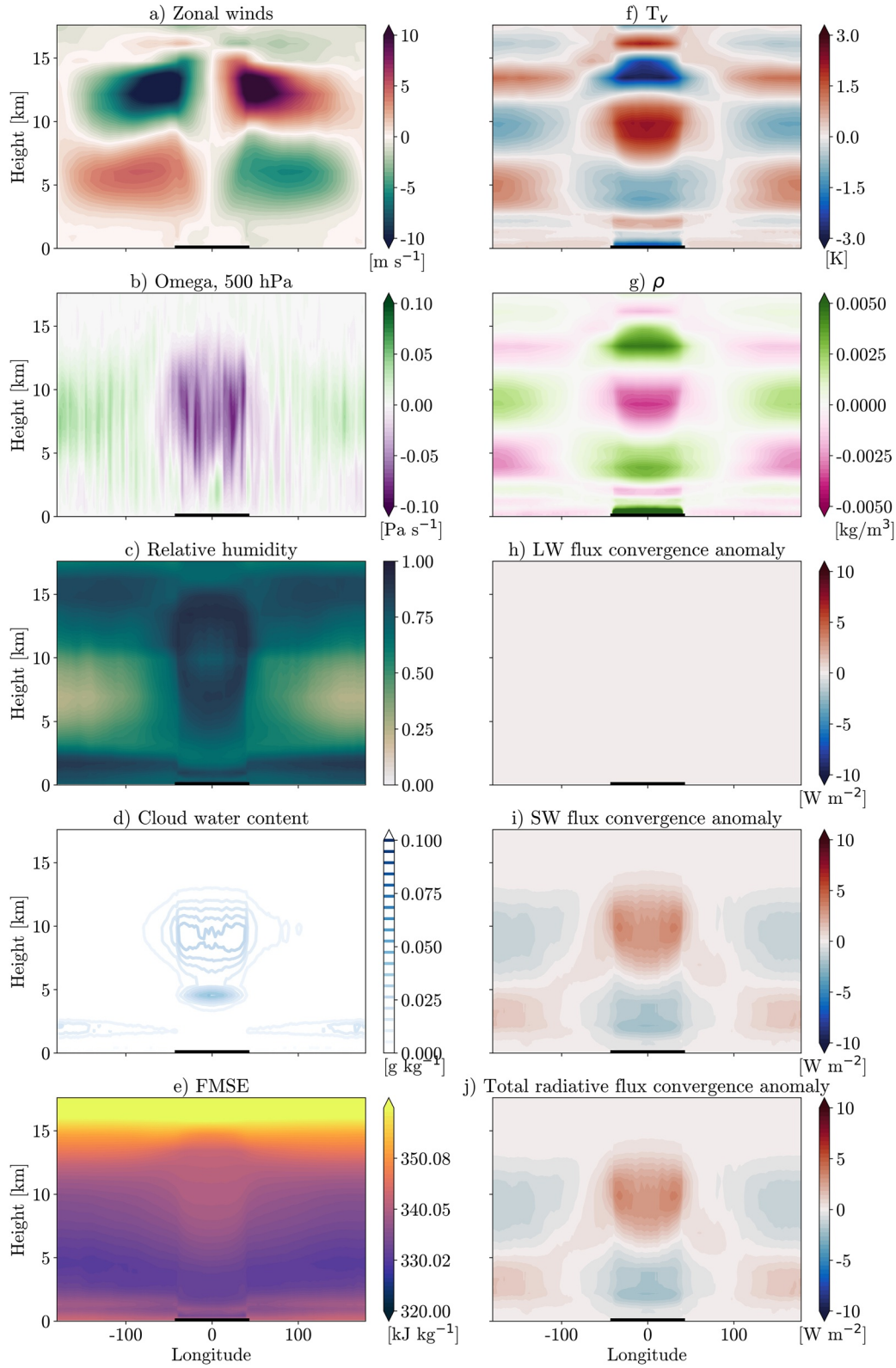

Figure 8. (a) Zonal winds, (b) Omega, (c) Relative humidity, (d) Cloud water content, (e) frozen moist static energy anomaly, (f) Virtual temperature anomaly, (g) Density anomaly, (h) Longwave radiative heating anomaly, (i) Shortwave radiative heating anomaly, and (j) Total radiative flux convergence anomaly. Plots are zonal slices taken at latitude = 0°, averaged over days 100–720 of the Land-HomogLW simulation. Island is located between longitudes ±40°, as indicated by thick black line. Anomalies are calculated from the horizontal mean.

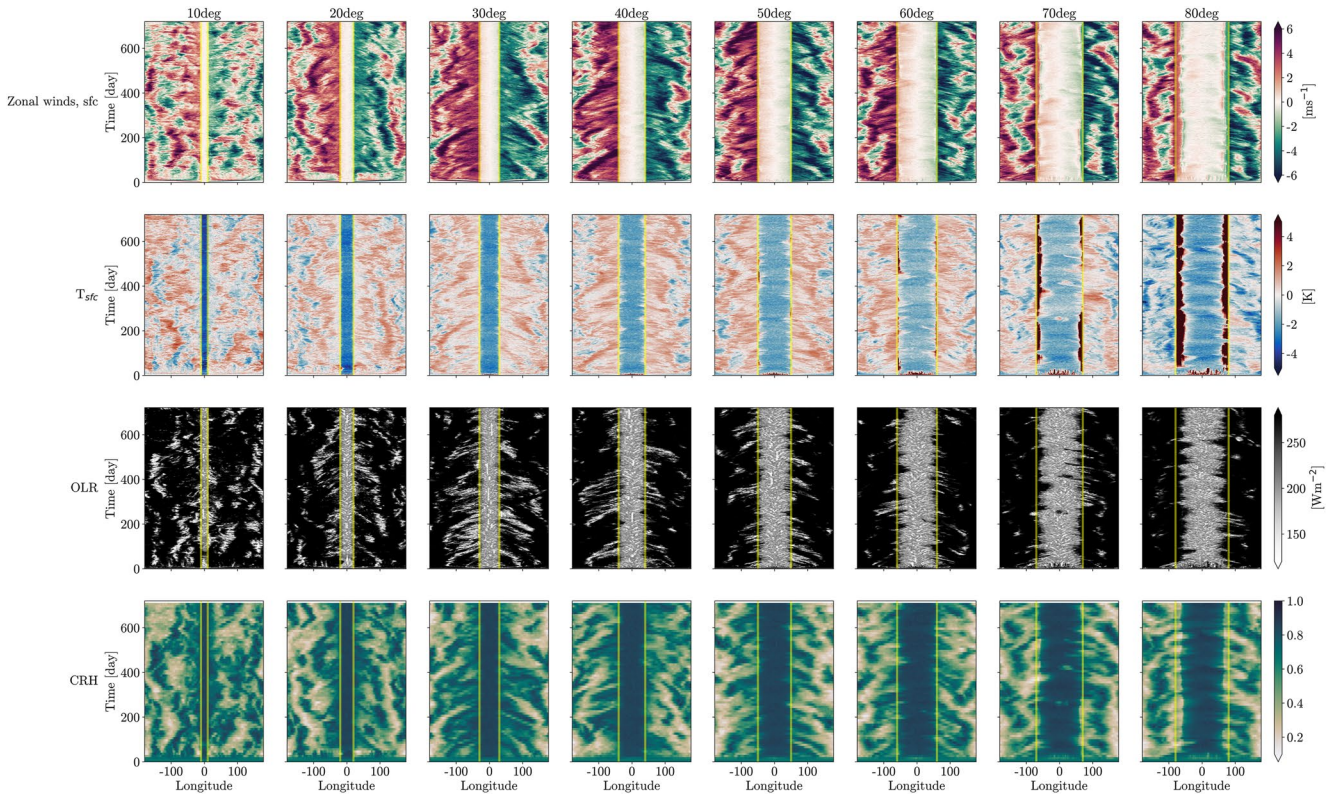

Figure 9. Hovmöller plots of (a–h) Surface zonal winds, (i–p) Near-surface temperature anomaly, (q–x) Outgoing longwave radiation, (y–Ff) Column relative humidity for 720 days radiative-convective equilibrium simulations with different land sizes. Land sizes increase from 10° (column 1) to 80° (column 8) in 10° increments. Anomalies are calculated from the horizontal mean.

outside of the island area, this leads to a maximum cluster size of $\mathcal{O}(10,000km)$, approximately the diameter of the 50° island. Matsugishi and Satoh (2022) investigated the natural length scale of convective aggregation in global models, and at an SST of 305K they estimated this to be approximately 2,000 km. Yang (2018b) also found that a typical length-scale of self-aggregation is $\mathcal{O}(2000km)$. Our results find a much larger size of convective cluster, however this is not a "natural" length scale, but instead a length scale due to the forcing presence of the island. Thus, it appears that when an inhomogeneity forces convection to aggregate, it can lead to an increase in the length scale of aggregation. Interestingly, the typical scale of the MJO, a phenomenon that has previously been linked to convective aggregation (Arnold & Randall, 2015; Khairoutdinov & Emanuel, 2018), is also $\mathcal{O}(10,000km)$, potentially indicating a relationship between our work and large-scale aggregation in the real world. Therefore, we recommend further work investigates aggregation length scales, particularly in models with increasing complexity, as our results indicate that forcings which are often excluded from more idealized aggregation studies could have a large impact on the spatial scale of organization.

4. Discussion and Conclusions

Using the ICON GCM, we ran RCE experiments which included a large, continentally sized island to investigate how the inclusion of land affects the phenomenon of convective aggregation. The island here represents a tropical rainforest-like land mass, with no elevation and no large-scale imposed winds, surrounded by a constant SST of 305K.

We showed that the inclusion of an idealized island in these global RCE simulations causes the convection to aggregate persistently over the island. This aggregation takes approximately 5–10 days to form spatially, however, it takes closer to 70 days for the model to reach statistical equilibrium, and therefore for the maximum degree of aggregation to be reached. The aggregation in these simulations causes similar domain-mean effects as self-aggregation has been shown to have before. This includes a domain-mean warming, free-tropospheric

drying and a reduction in the high cloud amount comparatively to a non-aggregated simulation (e.g., Bretherton et al., 2005; Coppin & Bony, 2015; Cronin & Wing, 2017; Wing & Cronin, 2016). One key difference between self-aggregation, and this land-forced aggregation is the domain-mean temperature profile. As in Cronin et al. (2015), we find that aggregation over the island causes a large increase in the domain-mean temperature, much greater than the temperature increase seen in an aquaplanet self-aggregated simulation (Figure 3). This is due to a warmer cloud-base temperature in the land simulation, which drives the convection onto a warmer moist adiabat. This warmer moist adiabat is then propagated to the rest of the domain through convectively triggered gravity waves. The similarity of our results to Cronin et al. (2015) occur because the soil on our island rapidly becomes saturated, as is typical for tropical rainforests (Nepstad et al., 1994; Schenk & Jackson, 2005), thus locking the simulation in a radiative-limited flux regime, rather than a soil moisture limited one. Soil is therefore never able to dry and induce the low-level circulation reversal as seen in Hohenegger and Stevens (2018). In the more complex modeling framework of TRACMIP (Voigt et al., 2016), inclusion of an idealized continent drove a domain-mean cooling across all models. Their simulation design included a zonally symmetric, meridional SST gradient, slab ocean, and seasonally varying insolation. The main driver of this cooling in their experiments was the development of a large cold "tongue" to the west of the continent due to low-level advection from the "winter" portion of the continent. Whilst originally seasonally driven, this anomaly develops into a persistent annual feature due to feedbacks between the cold SST, atmospheric humidity, and temperature (Biasutti et al., 2021). Thus, despite significant differences between our study and TRACMIP, there are some similarities in the ability of the land to drive an initial perturbation, which can then be maintained through atmospheric feedbacks.

We showed that the circulation is initially triggered by a strong land-sea thermal contrast at the surface, driving a sea-breeze circulation, which has been shown to have important impacts on convection and precipitation over tropical islands, particularly in the Maritime Continent (Leutwyler & Hohenegger, 2021; Miller et al., 2003). In our simulations, the sea-breeze circulation triggers convection (Carbone et al., 2000; Crook, 2001; Kingsmill, 1995), first at the edge of the island before being triggered increasingly inland. This convection then incites a gravity wave, moving at approximately 30 m s^{-1} outwards from the island. Gravity wave induced subsidence dries the columns furthest away from the island, and saturated cloud detrainment in the vicinity of the convection moistens locally, which forms large gradients in the CRH (Lane & Reeder, 2001). Once these atmospheric moisture gradients form, radiative feedbacks start to dominate the maintenance of the circulation through the strong longwave heating within the cloud layer. These longwave anomalies drive a strong virtual temperature gradient in the lower troposphere, which then causes the radiatively driven circulation to persist throughout the simulation, despite negative near-surface temperature anomalies over the island.

We tested these hypotheses by horizontally homogenizing the longwave feedbacks. In contrast to the results above, these sensitivity tests showed that convection remains organized, with persistent convection over the island. However, convection forming over the ocean also happens more regularly than in our Land-NoHomog simulation. Additionally, surface convergence is no longer maintained. Instead, shortwave heating drives a mid-tropospheric virtual temperature anomaly which causes a large-scale thermally driven circulation, although one that is elevated above the boundary layer. In the absence of boundary layer convergence, the advection of FMSE is also reduced, which Muller and Bony (2015) found was essential for aggregation. Here, we see that convection can still be organized spatially, but without this upgradient advection, the organization no longer drives large-scale climatological changes. Due to this, we have concluded that there is an additional, different mechanism which is also crucial for the aggregation alongside the longwave feedbacks.

Finally, it is difficult to quantify whether the Land-HomogLW simulation is aggregated or not—it could be labeled as either based on how we choose to define aggregation. Is convective self-aggregation simply the geometrical organization of convection, or is it the geometrical organization combined with large-scale climatological impacts, such as the broadening of the moisture field? Nevertheless, we have shown here that by removing the horizontal gradients in longwave radiative fluxes, convection is less spatially organized with increased oceanic convection compared with the Land-NoHomog simulation. However, convection is still being consistently triggered over the island in the absence of horizontal gradients in the longwave radiative fluxes and thus these fluxes cannot be the only necessary mechanism of organization. This mechanism should be further investigated in future studies to gain an improved understanding on the interactions between land and convective aggregation.

These results are of course subject to the idealizations made in this study—for example, would the inclusion of a diurnal cycle allow for a nocturnal reversal of the land-sea breeze, thus disrupting the large-scale, radiatively

driven circulation? Cronin et al. (2015) found that the diurnal cycle-induced nocturnal surface cooling was insufficient to destabilize the deep overturning circulation, leading to a time-mean, island-centered circulation, although their study excluded the potential effects of soil moisture. We postulate that, given our land-surface remains cooler through our simulations once aggregated, and given the long timescales associated with soil drying (e.g., Bruno et al., 2006; Teuling et al., 2006), it is likely that in the time-mean our results would still hold in the presence of a diurnal cycle. However, confirming this requires further work outside the scope of this experiment, and we recommend this as an avenue for future study.

The results we have presented in this paper mostly scale with island size, until islands have a radius greater than 50° with the large-scale circulation roughly increasing in extent with island size, and the resulting convective cluster always covering the entire island. For all experiments, convection covers roughly 25% of the globe, however with increasing island size, this convection is increasingly centered on the island. This means that, for the largest island sizes, the convective cluster is no longer able to cover the whole island. This work thus points to a maximum size of convective clustering in a global domain, something that has been a recent topic of interest (Arnold & Putman, 2018; Beucler & Cronin, 2019; Yang, 2018b). We highlight that the modeling design used in this study could be useful in investigating the spatial scale of aggregation. We therefore encourage future work to develop of a theoretical understanding of the scale of aggregation, especially in more complex atmospheres than standard RCE.

We present this paper as an investigation of the impacts land-sea contrasts have on convective aggregation in a global configuration, and provide it as a useful addition to the growing literature on connecting idealized aggregation studies to the manifestation of real world convective organization (e.g., Arnold & Randall, 2015; Becker & Wing, 2020; Beucler et al., 2020; Bony et al., 2020; Hohenegger & Stevens, 2016, 2018; Müller & Hohenegger, 2020; Muller & Romps, 2018; Shamekh et al., 2020a; Tompkins, 2001a). We have shown that, whilst the shape and scale of aggregation change when a continentally sized island is included in an idealized RCE world, many of the features of aggregation remain the same, including its effects on the large-scale environment. There are also similarities between the mechanisms of more idealized self-aggregation, and aggregation in the presence of a land-sea contrast. However, there are crucial differences in the mechanisms, which should be further explored. It can be difficult to draw conclusions on how results shown in this and other similar papers might be manifested in the real world, due to the experiment's highly idealized configuration. To that end, there are many extensions to this paper that we feel will help to further elucidate the relationship between idealized aggregation and it's real world manifestations, including investigating the effects of the diurnal cycle, SST gradients and rotation on the results presented here.

Appendix A: Vegetation Sensitivity Test

To test the sensitivity of our results to the vegetation chosen, we have run an additional experiment where the land initial and boundary conditions are set to grass-like parameters instead of tropical rainforest ones. Typically, rainforests are characterized by greater evapotranspiration and roughness lengths and a lower albedo than other vegetation types (Shuttleworth, 1989). As shown in the results above, surface fluxes can have a large impact on convective and precipitation and thus these changes in surface parameters could also impact our results. In particular, we showed that the high surface fluxes, driven by the sensible heat flux in the first 3 days of the simulations triggered convection and thus determined the location of our aggregation.

For the following results we used the land parameters from the short grass experiment in Bell et al. (2015), with the JSBACH4 PFT flag 7, and loamy soil (FAO flag 3). A table listing the parameters for both the rainforest and grass experiment can be found in Table 1.

The results found in the main body of the paper mostly hold when the vegetation was changed to grass. Figure A1 shows the same fields as in Figure 4, but for our grass experiment. It is clear that, after the first 2 days, the two simulations are extremely similar. Similarly, we can examine the driving feedbacks derived from the FMSE variance budget for both experiments to again see very similar results (Figure A2). The main differences between the two experiments lies in the first 2 days of the 2 m temperature, the Bowen ratio, and thus the relative surface flux contribution from latent and sensible heat. Whilst in our rainforest experiment the land initially became far warmer than the surrounding oceans, here we see a weaker, though still positive temperature anomaly over land. There is also a much lower Bowen ratio over land for the grass experiment, although the surface enthalpy flux

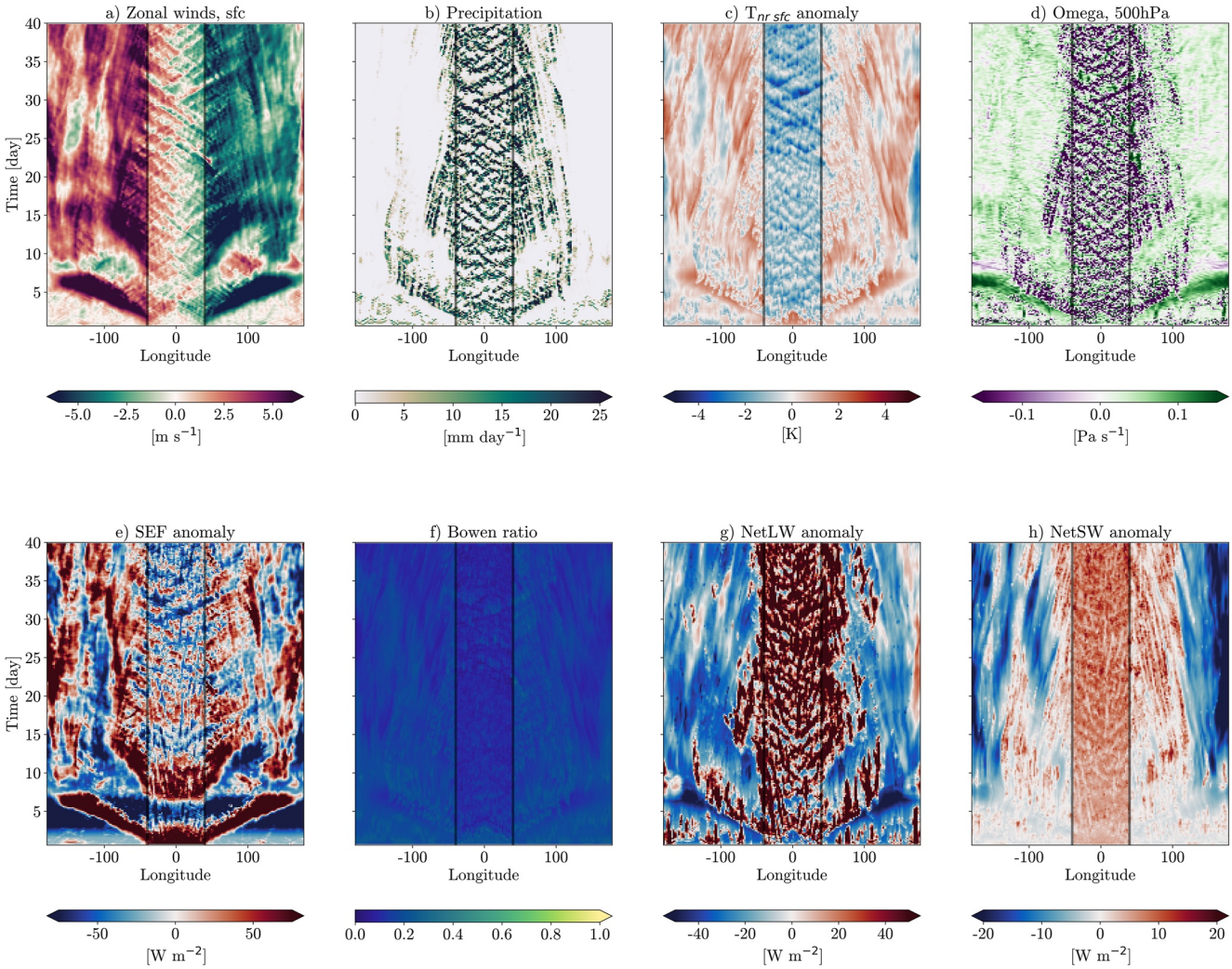

Figure A1. Hovmöller plots of (a) Surface zonal winds, (b) Precipitation, (c) Near-surface temperature anomaly, (d) Omega at 500 hPa, (e) surface enthalpy flux (latent heat flux [LHF] + sensible heat flux [SHF]) anomaly, (f) Bowen ratio (SHF/LHF), (g) NetLW anomaly, and (h) NetSW anomaly, over the first 40 days the simulation with grass vegetation, taken as a zonal slice through latitude = 0°. The black lines show the coasts of the island. NetLW and NetSW are the column longwave and shortwave radiative flux convergences, respectively. Anomalies are calculated from the horizontal mean.

anomaly is of a similar magnitude. This implies that, instead of the sensible heat fluxes initially driving the aggregation, here we see that it is the latent heat fluxes acting as a FMSE source over land. This is confirmed in the FMSE variance budget plots in Figure A2. Figure A2a shows that the surface flux feedbacks are again the main driver of aggregation in the first day with the longwave feedbacks dominating after that. Equally, Figure A2b confirms that it is the latent heat fluxes driving this surface flux feedback. Figure A1h shows that the NetSW anomaly is greater in the earliest few days than in the rainforest experiment (Figure 4h). This is due to the higher albedo of the grass vegetation which therefore reflects more of the incoming solar radiation while the island is cloud free at the start of the simulation. Thus, less shortwave is absorbed at the surface which is why we see a smaller near surface temperature anomaly and hence surface energy balance is reached by a lower Bowen ratio. After the first day, convection begins to be triggered over the island, and the same feedbacks as in the rainforest experiment, namely the longwave radiative fluxes, begin to dominate once more.

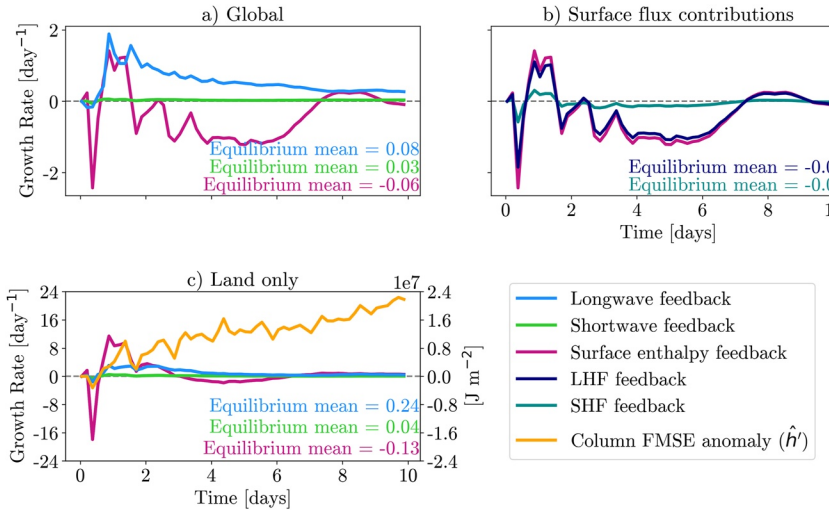

Figure A2. Timeseries of diabatic terms in frozen moist static energy variance budget (Equation 2) over first 10 days of the simulation with grass vegetation. (a) Averaged globally, (b) Globally averaged surface flux contributions, (c) averaged over the island only. Panel (c) also includes the land-averaged values of $\hat{h}'$, on the right-hand y-axis. Light blue lines show longwave feedback, green lines show shortwave feedback, pink lines show surface enthalpy feedback, navy blue lines shown latent heat flux feedback, teal lines show sensible heat flux feedback, orange line shows $\hat{h}'$. Mean values over days 90–180 (when the simulation is in equilibrium) of each feedback are given in the text on each plot (color of text corresponds to feedback line color).

Thus, even with different vegetation driving a different partitioning of the surface fluxes, we still see convective aggregation preferably forming over the island in our simulations. The location of this aggregation is driven by surface fluxes, with the surface enthalpy feedback being the dominant term in the FMSE variance budget in the first 1–2 days of both grass and rainforest simulations. After this initial period, the longwave feedbacks become the strongest feedback.

Data Availability Statement

All data is freely available in NetCDF format online in the CEDA archive at http://dx.doi.org/10.5285/3c42e6131ae44b9793648065dc4162b4.

Acknowledgments
We would like to thank Adrian Tompkins, Cornelia Klein, and Simona Bordoni whose comments helped to improve the manuscript significantly. B. D. acknowledges funding from the Natural Environment Research Council, Oxford DTP, Award NE/L002612/1. G. D. is supported by the Israeli Science Foundation Grant (1419/21). G. D, P. S., and R. H. were also supported by the European Research Council (ERC) project constRaining the EffeCts of Aerosols on Precipitation (RECAP) under the European Union's Horizon 2020 research and innovation programme with Grant 724602. P. S. additionally acknowledges funding from the FORCeS and NextGEMs projects under the European Union's Horizon 2020 research program with Grants 821205 and 101003470, respectively. Computations and data processing have been performed on the ARCHER2 and JASMIN computing facilities. We also thank Cathy Hohenegger and Andrew Williams for the fruitful discussions during the preparation of this paper. We thank the Centre for Environmental Data Analysis (CEDA) Archive for hosting our model output data.

References

Arnold, N. P., & Putman, W. M. (2018). Nonrotating convective self-aggregation in a limited area AGCM. *Journal of Advances in Modeling Earth Systems*, *10*(4), 1029–1046. https://doi.org/10.1002/2017ms001218

Arnold, N. P., & Randall, D. A. (2015). Global-scale convective aggregation: Implications for the Madden-Julian Oscillation. *Journal of Advances in Modeling Earth Systems*, *7*(4), 1499–1518. https://doi.org/10.1002/2015MS000498

Becker, T., & Wing, A. A. (2020). Understanding the extreme spread in climate sensitivity within the radiative-convective equilibrium model intercomparison project. *Journal of Advances in Modeling Earth Systems*, *12*(10), e2020MS002165. https://doi.org/10.1029/2020MS002165

Bell, J. P., Tompkins, A. M., Bouka-Biona, C., & Sanda, I. S. (2015). A process-based investigation into the impact of the Congo basin deforestation on surface climate. *Journal of Geophysical Research: Atmospheres*, *120*(12), 5721–5739. https://doi.org/10.1002/2014JD022586

Beucler, T., & Cronin, T. (2019). A budget for the size of convective self-aggregation. *Quarterly Journal of the Royal Meteorological Society*, *145*(720), 947–966. https://doi.org/10.1002/qj.3468

Beucler, T., Leutwyler, D., & Windmiller, J. M. (2020). Quantifying convective aggregation using the tropical moist margin's length. *Journal of Advances in Modeling Earth Systems*, *12*(10), e2020MS002092. https://doi.org/10.1029/2020MS002092

Biasutti, M., Russotto, R. D., Voigt, A., & Blackmon-Luca, C. C. (2021). The effect of an equatorial continent on the tropical rain belt. Part I: Annual mean changes in the ITCZ. *Journal of Climate*, *34*(14), 5813–5828. https://doi.org/10.1175/JCLI-D-20-0739.1

Bony, S., Semie, A., Kramer, R. J., Soden, B., Tompkins, A. M., & Emanuel, K. A. (2020). Observed modulation of the tropical radiation budget by deep convective organization and lower-tropospheric stability. *AGU Advances*, *1*(3), e2019AV000155. https://doi.org/10.1029/2019AV000155

Bretherton, C. S., Blossey, P. N., & Khairoutdinov, M. (2005). An energy-balance analysis of deep convective self-aggregation above uniform SST. *Journal of the Atmospheric Sciences*, *62*(12), 4273–4292. https://doi.org/10.1175/JAS3614.1

Bruno, R. D., Da Rocha, H. R., De Freitas, H. C., Goulden, M. L., & Miller, S. D. (2006). Soil moisture dynamics in an eastern Amazonian tropical forest. *Hydrological Processes: International Journal*, *20*(12), 2477–2489. https://doi.org/10.1002/hyp.6211

Carbone, R. E., Wilson, J. W., Keenan, T. D., & Hacker, J. M. (2000). Tropical island convection in the absence of significant topography. Part I: Life cycle of diurnally forced convection. *Monthly Weather Review*, *128*(10), 3459–3480. https://doi.org/10.1175/1520-0493(2000)128⟨3459:TICITA⟩2.0.CO;2

Coppin, D., & Bellon, G. (2019). Physical mechanisms controlling the offshore propagation of convection in the tropics: 1. Flat island. *Journal of Advances in Modeling Earth Systems*, *11*(9), 3042–3056. https://doi.org/10.1029/2019MS001793

Coppin, D., & Bony, S. (2015). Physical mechanisms controlling the initiation of convective self-aggregation in a general circulation model. *Journal of Advances in Modeling Earth Systems*, *7*(4), 2060–2078. https://doi.org/10.1002/2015MS000571

Cronin, T. W., Emanuel, K. A., & Molnar, P. (2015). Island precipitation enhancement and the diurnal cycle in radiative-convective equilibrium. *Quarterly Journal of the Royal Meteorological Society*, *141*(689), 1017–1034. https://doi.org/10.1002/qj.2443

Cronin, T. W., & Wing, A. A. (2017). Clouds, circulation, and climate sensitivity in a radiative-convective equilibrium channel model. *Journal of Advances in Modeling Earth Systems*, *9*(8), 2883–2905. https://doi.org/10.1002/2017MS001111

Crook, N. A. (2001). Understanding hector: The dynamics of island thunderstorms. *Monthly Weather Review*, *129*(6), 1550–1563. https://doi.org/10.1175/1520-0493(2001)129⟨1550:UHTDOI⟩2.0.CO;2

Davis, C. A. (2015). The formation of moist vortices and tropical cyclones in idealized simulations. *Journal of the Atmospheric Sciences*, *72*(9), 3499–3516. https://doi.org/10.1175/jas-d-15-0027.1

Dingley, B., Dagan, G., & Stier, P. (2021). Forcing convection to aggregate using diabatic heating perturbations. *Journal of Advances in Modeling Earth Systems*, *13*(10), e2021MS002579. https://doi.org/10.1029/2021ms002579

Findell, K. L., & Eltahir, E. A. B. (2003). Atmospheric controls on soil moisture–boundary layer interactions. Part I: Framework development. *Journal of Hydrometeorology*, *4*(3), 552–569. https://doi.org/10.1175/1525-7541(2003)004⟨0552:ACOSML⟩2.0.CO;2

Gentine, P., Holtslag, A. A. M., D'Andrea, F., & Ek, M. (2013). Surface and atmospheric controls on the onset of moist convection over land. *Journal of Hydrometeorology*, *14*(5), 1443–1462. https://doi.org/10.1175/JHM-D-12-0137.1

Giorgetta, M. A., Brokopf, R., Crueger, T., Esch, M., Fiedler, S., Helmert, J., et al. (2018). ICON-A, the atmosphere component of the ICON Earth system model: I. Model description. *Journal of Advances in Modeling Earth Systems*, *10*(7), 1613–1637. https://doi.org/10.1029/2017MS001242

Grabowski, W. W., & Moncrieff, M. W. (2004). Moisture–convection feedback in the tropics. *Quarterly Journal of the Royal Meteorological Society: A Journal of the Atmospheric Sciences, Applied Meteorology and Physical Oceanography*, *130*(604), 3081–3104. https://doi.org/10.1256/qj.03.135

Hagemann, S. (2002). *An improved land surface parameter dataset for global and regional climate models* (Tech. Rep.). Max Planck Institute for Meteorology.

Held, I. M., Hemler, R. S., & Ramaswamy, V. (1993). Radiative-convective equilibrium with explicit two-dimensional moist convection. *Journal of the Atmospheric Sciences*, *50*(23), 3909–3927. https://doi.org/10.1175/1520-0469(1993)050⟨3909:RCEWET⟩2.0.CO;2

Hohenegger, C., & Stevens, B. (2016). Coupled radiative convective equilibrium simulations with explicit and parameterized convection. *Journal of Advances in Modeling Earth Systems*, *8*(3), 1468–1482. https://doi.org/10.1002/2016ms000666

Hohenegger, C., & Stevens, B. (2018). The role of the permanent wilting point in controlling the spatial distribution of precipitation. *Proceedings of the National Academy of Sciences of the United States of America*, *115*(22), 5692–5697. https://doi.org/10.1073/pnas.1718842115

Holloway, C. E., & Woolnough, S. J. (2016). The sensitivity of convective aggregation to diabatic processes in idealized radiative-convective equilibrium simulations. *Journal of Advances in Modeling Earth Systems*, *8*(1), 166–195. https://doi.org/10.1002/2015ms000511

Jakob, C., Singh, M. S., & Jungandreas, L. (2019). Radiative convective equilibrium and organized convection: An observational perspective. *Journal of Geophysical Research: Atmospheres*, *124*(10), 5418–5430. https://doi.org/10.1029/2018JD030092

Jungclaus, J. H., Lorenz, S. J., Schmidt, H., Brovkin, V., Brüggemann, N., Chegini, F., et al. (2022). The ICON Earth system model version 1.0. *Journal of Advances in Modeling Earth Systems*, *14*(4), e2021MS002813. https://doi.org/10.1029/2021MS002813

Khairoutdinov, M. F., & Emanuel, K. A. (2013). Rotating radiative-convective equilibrium simulated by a cloud-resolving model. *Journal of Advances in Modeling Earth Systems*, *5*(4), 816–825. https://doi.org/10.1002/2013ms000253

Khairoutdinov, M. F., & Emanuel, K. A. (2018). Intraseasonal variability in a cloud-permitting near-global equatorial aquaplanet model. *Journal of the Atmospheric Sciences*, *75*(12), 4337–4355. https://doi.org/10.1175/jas-d-18-0152.1

Kingsmill, D. E. (1995). Convection initiation associated with a sea-breeze front, a gust front, and their collision. *Monthly Weather Review*, *123*(10), 2913–2933. https://doi.org/10.1175/1520-0493(1995)123⟨2913:CIAWAS⟩2.0.CO;2

Koster, R. D., Dirmeyer, P. A., Guo, Z., Bonan, G., Chan, E., Cox, P., et al. (2004). Regions of strong coupling between soil moisture and precipitation. *Science*, *305*(5687), 1138–1140. https://doi.org/10.1126/science.1100217

Lane, T. P., & Reeder, M. J. (2001). Convectively generated gravity waves and their effect on the cloud environment. *Journal of the Atmospheric Sciences*, *58*(16), 2427–2440. https://doi.org/10.1175/1520-0469(2001)058<2427:cggwat>2.0.co;2

Leutwyler, D., & Hohenegger, C. (2021). Weak cooling of the troposphere by tropical islands in simulations of the radiative-convective equilibrium. *Quarterly Journal of the Royal Meteorological Society*, *147*(736), 1788–1800. https://doi.org/10.1002/qj.3995

Lohmann, U., & Roeckner, E. (1996). Design and performance of a new cloud microphysics scheme developed for the ECHAM general circulation model. *Climate Dynamics*, *12*(8), 557–572. https://doi.org/10.1007/BF00207939

Madden, R. A., & Julian, P. R. (1994). Observations of the 40–50-day tropical oscillation—A review. *Monthly Weather Review*, *122*(5), 814–837. https://doi.org/10.1175/1520-0493(1994)122⟨0814:OOTDTO⟩2.0.CO;2

Manabe, S., & Wetherald, R. T. (1967). Thermal equilibrium of the atmosphere with a given distribution of relative humidity. *Journal of the Atmospheric Sciences*, *24*(3), 241–259. https://doi.org/10.1175/1520-0469(1967)024⟨0241:TEOTAW⟩2.0.CO;2

Matsugishi, S., & Satoh, M. (2022). Sensitivity of the horizontal scale of convective self-aggregation to sea surface temperature in radiative convective equilibrium experiments using a global nonhydrostatic model. *Journal of Advances in Modeling Earth Systems*, *14*(5), e2021MS002636. https://doi.org/10.1029/2021MS002636

Miller, S. T. K., Keim, B. D., Talbot, R. W., & Mao, H. (2003). Sea breeze: Structure, forecasting, and impacts. *Reviews of Geophysics*, *41*(3), 1011. https://doi.org/10.1029/2003RG000124

Muller, C. J., & Bony, S. (2015). What favors convective aggregation and why? *Geophysical Research Letters*, *42*(13), 5626–5634. https://doi.org/10.1002/2015GL064260

Muller, C. J., & Held, I. (2012). Detailed investigation of the self-aggregation of convection in cloud-resolving simulations. *Journal of the Atmospheric Sciences*, *69*(8), 2551–2565. https://doi.org/10.1175/JAS-D-11-0257.1

Muller, C. J., & Romps, D. M. (2018). Acceleration of tropical cyclogenesis by self-aggregation feedbacks. *Proceedings of the National Academy of Sciences of the United States of America*, *115*(12), 2930–2935. https://doi.org/10.1073/pnas.1719967115

Müller, S. K., & Hohenegger, C. (2020). Self-aggregation of convection in spatially varying sea surface temperatures. *Journal of Advances in Modeling Earth Systems*, *12*(1), e2019MS001698. https://doi.org/10.1029/2019ms001698

Naumann, A. K., Stevens, B., Hohenegger, C., & Mellado, J. P. (2017). A conceptual model of a shallow circulation induced by prescribed low-level radiative cooling. *Journal of the Atmospheric Sciences*, *74*(10), 3129–3144. https://doi.org/10.1175/jas-d-17-0030.1

Nepstad, D. C., de Carvalho, C. R., Davidson, E. A., Jipp, P. H., Lefebvre, P. A., Negreiros, G. H., et al. (1994). The role of deep roots in the hydrological and carbon cycles of Amazonian forests and pastures. *Nature*, *372*(6507), 666–669. https://doi.org/10.1038/372666a0

Nordeng, T.-E. (1994). Extended versions of the convective parametrization scheme at ECMWF and their impact on the mean and transient activity of the model in the tropics. *Research Department Technical Memorandum*, *206*, 1–41. https://doi.org/10.21957/e34xwhysw
Popke, D., Stevens, B., & Voigt, A. (2013). Climate and climate change in a radiative-convective equilibrium version of ECHAM6. *Journal of Advances in Modeling Earth Systems*, *5*, 1–14. https://doi.org/10.1029/2012MS000191@10.1002/(ISSN)1942-2466.MPIESM1
Popp, M., & Bony, S. (2019). Stronger zonal convective clustering associated with a wider tropical rain belt. *Nature Communications*, *10*(1), 1–12. https://doi.org/10.1038/s41467-019-13645-w
Reick, C. H., Gayler, V., Goll, D., Hagemann, S., Heidkamp, M., Nabel, J. E. M. S., et al. (2021). *JSBACH 3-the land component of the MPI earth system model: Documentation of version 3.2* (Tech. Rep.). Max Planck Institute for Meteorology.
Reick, C. H., Raddatz, T., Brovkin, V., & Gayler, V. (2013). Representation of natural and anthropogenic land cover change in MPI-ESM. *Journal of Advances in Modeling Earth Systems*, *5*(3), 459–482. https://doi.org/10.1002/jame.20022
Robe, F. R., & Emanuel, K. A. (2001). The effect of vertical wind shear on radiative–convective equilibrium states. *Journal of the Atmospheric Sciences*, *58*(11), 1427–1445. https://doi.org/10.1175/1520-0469(2001)058<1427:teovws>2.0.co;2
Roca, R., & Fiolleau, T. (2020). Extreme precipitation in the tropics is closely associated with long-lived convective systems. *Communications Earth & Environment*, *1*(1), 1–6. https://doi.org/10.1038/s43247-020-00015-4
Sato, T., Miura, H., Satoh, M., Takayabu, Y. N., & Wang, Y. (2009). Diurnal cycle of precipitation in the tropics simulated in a global cloud-resolving model. *Journal of Climate*, *22*(18), 4809–4826. https://doi.org/10.1175/2009JCLI2890.1
Schenk, H. J., & Jackson, R. B. (2005). Mapping the global distribution of deep roots in relation to climate and soil characteristics. *Geoderma*, *126*(1–2), 129–140. https://doi.org/10.1016/j.geoderma.2004.11.018
Seneviratne, S. I., Corti, T., Davin, E. L., Hirschi, M., Jaeger, E. B., Lehner, I., et al. (2010). Investigating soil moisture–climate interactions in a changing climate: A review. *Earth-Science Reviews*, *99*(3–4), 125–161. https://doi.org/10.1016/j.earscirev.2010.02.004
Seneviratne, S. I., Lüthi, D., Litschi, M., & Schär, C. (2006). Land–atmosphere coupling and climate change in Europe. *Nature*, *443*(7108), 205–209. https://doi.org/10.1038/nature05095
Shamekh, S., Muller, C. J., Duvel, J.-P., & d'Andrea, F. (2020a). How do ocean warm anomalies favor the aggregation of deep convective clouds? *Journal of the Atmospheric Sciences*, *77*(11), 3733–3745. https://doi.org/10.1175/jas-d-18-0369.1
Shamekh, S., Muller, C. J., Duvel, J.-P., & d'Andrea, F. (2020b). Self-aggregation of convective clouds with interactive sea surface temperature. *Journal of Advances in Modeling Earth Systems*, *12*(11), e2020MS002164. https://doi.org/10.1029/2020MS002164
Shuttleworth, W. J. (1989). Micrometeorology of temperate and tropical forest. *Philosophical Transactions of the Royal Society of London B Biological Sciences*, *324*(1223), 299–334. https://doi.org/10.1098/rstb.1989.0050
Sobel, A. H., Nilsson, J., & Polvani, L. M. (2001). The weak temperature gradient approximation and balanced tropical moisture waves. *Journal of the Atmospheric Sciences*, *58*(23), 3650–3665. https://doi.org/10.1175/1520-0469(2001)058⟨3650:TWTGAA⟩2.0.CO;2
Stephens, G. L., Van Den Heever, S., & Pakula, L. (2008). Radiative–convective feedbacks in idealized states of radiative–convective equilibrium. *Journal of the Atmospheric Sciences*, *65*(12), 3899–3916. https://doi.org/10.1175/2008jas2524.1
Stevens, B., Giorgetta, M., Esch, M., Mauritsen, T., Crueger, T., Rast, S., et al. (2013). Atmospheric component of the MPI-M Earth system model: ECHAM6. *Journal of Advances in Modeling Earth Systems*, *5*(2), 146–172. https://doi.org/10.1002/jame.20015
Sundqvist, H., Berge, E., & Kristjánsson, J. E. (1989). Condensation and cloud parameterization studies with a mesoscale numerical weather prediction model. *Monthly Weather Review*, *117*(8), 1641–1657. https://doi.org/10.1175/1520-0493(1989)117⟨1641:CACPSW⟩2.0.CO;2
Taylor, C. M., de Jeu, R. A. M., Guichard, F., Harris, P. P., & Dorigo, W. A. (2012). Afternoon rain more likely over drier soils. *Nature*, *489*(7416), 423–426. https://doi.org/10.1038/nature11377
Teuling, A. J., Seneviratne, S. I., Williams, C., & Troch, P. A. (2006). Observed timescales of evapotranspiration response to soil moisture. *Geophysical Research Letters*, *33*(23), L23403. https://doi.org/10.1029/2006GL028178
Tiedtke, M. (1989). A comprehensive mass flux scheme for cumulus parameterization in large-scale models. *Monthly Weather Review*, *117*(8), 1779–1800. https://doi.org/10.1175/1520-0493(1989)117⟨1779:ACMFSF⟩2.0.CO;2
Tobin, I., Bony, S., & Roca, R. (2012). Observational evidence for relationships between the degree of aggregation of deep convection, water vapor, surface fluxes, and radiation. *Journal of Climate*, *25*(20), 6885–6904. https://doi.org/10.1175/JCLI-D-11-00258.1
Tompkins, A. M. (2001a). On the relationship between tropical convection and sea surface temperature. *Journal of Climate*, *14*(5), 633–637. https://doi.org/10.1175/1520-0442(2001)014<0633:otrbtc>2.0.co;2
Tompkins, A. M. (2001b). Organization of tropical convection in low vertical wind shears: The role of cold pools. *Journal of the Atmospheric Sciences*, *58*(13), 1650–1672. https://doi.org/10.1175/1520-0469(2001)058<1650:ootcil>2.0.co;2
Tompkins, A. M., & Craig, G. C. (1998). Radiative–convective equilibrium in a three-dimensional cloud-ensemble model. *Quarterly Journal of the Royal Meteorological Society*, *124*(550), 2073–2097. https://doi.org/10.1002/qj.49712455013
Tompkins, A. M., & Semie, A. G. (2021). Impact of a mixed ocean layer and the diurnal cycle on convective aggregation. *Journal of Advances in Modeling Earth Systems*, *13*(12), e2020MS002186. https://doi.org/10.1029/2020MS002186
Voigt, A., Biasutti, M., Scheff, J., Bader, J., Bordoni, S., Codron, F., et al. (2016). The tropical rain belts with an annual cycle and a continent model intercomparison project: TRACMIP. *Journal of Advances in Modeling Earth Systems*, *8*(4), 1868–1891. https://doi.org/10.1002/2016MS000748
Wang, S., & Sobel, A. H. (2017). Factors controlling rain on small tropical islands: Diurnal cycle, large-scale wind speed, and topography. *Journal of the Atmospheric Sciences*, *74*(11), 3515–3532. https://doi.org/10.1175/JAS-D-16-0344.1
Wing, A. A., Camargo, S. J., & Sobel, A. H. (2016). Role of radiative–convective feedbacks in spontaneous tropical cyclogenesis in idealized numerical simulations. *Journal of the Atmospheric Sciences*, *73*(7), 2633–2642. https://doi.org/10.1175/jas-d-15-0380.1
Wing, A. A., & Cronin, T. W. (2016). Self-aggregation of convection in long channel geometry. *Quarterly Journal of the Royal Meteorological Society*, *142*(694), 1–15. https://doi.org/10.1002/qj.2628
Wing, A. A., & Emanuel, K. A. (2014). Physical mechanisms controlling self-aggregation of convection in idealized numerical modeling simulations. *Journal of Advances in Modeling Earth Systems*, *6*(1), 59–74. https://doi.org/10.1002/2013MS000269
Wing, A. A., Emanuel, K. A., Holloway, C. E., & Muller, C. J. (2017). Convective self-aggregation in numerical simulations: A review. In *Shallow clouds, water vapor, circulation, and climate sensitivity* (pp. 1–25). https://doi.org/10.1007/978-3-319-77273-8_1
Wing, A. A., Reed, K. A., Satoh, M., Stevens, B., Bony, S., & Ohno, T. (2018). Radiative–convective equilibrium model intercomparison project. *Geoscientific Model Development*, *11*(2), 793–813. https://doi.org/10.5194/gmd-11-793-2018
Wing, A. A., Stauffer, C. L., Becker, T., Reed, K. A., Ahn, M.-S., Arnold, N. P., et al. (2020). Clouds and convective self-aggregation in a multi-model ensemble of radiative-convective equilibrium simulations. *Journal of Advances in Modeling Earth Systems*, *12*(9), e2020MS002138. https://doi.org/10.1029/2020ms002138
Yang, D. (2018a). Boundary layer diabatic processes, the virtual effect, and convective self-aggregation. *Journal of Advances in Modeling Earth Systems*, *10*(9), 2163–2176. https://doi.org/10.1029/2017MS001261

Yang, D. (2018b). Boundary layer height and buoyancy determine the horizontal scale of convective self-aggregation. *Journal of the Atmospheric Sciences*, *75*(2), 469–478. https://doi.org/10.1175/jas-d-17-0150.1

Zängl, G., Reinert, D., Rípodas, P., & Baldauf, M. (2015). The ICON (ICOsahedral Non-hydrostatic) modelling framework of DWD and MPI-M: Description of the non-hydrostatic dynamical core. *Quarterly Journal of the Royal Meteorological Society*, *141*(687), 563–579. https://doi.org/10.1002/qj.2378